NASA TECHNICAL MEMORANDUM

NASA TM X-64890

(NASA-TM-X-64890) STATUS OF FLOW SEPARATION PREDICTION IN LIQUID PROPELLANT ROCKET NOZZLES (NASA) 69 p HC $4.25 CSCL 21H

N75-12061

Unclas
G3/20 02859

STATUS OF FLOW SEPARATION PREDICTION IN LIQUID PROPELLANT ROCKET NOZZLES

By Robert H. Schmucker
Structures and Propulsion Laboratory

November 1974

NASA

George C. Marshall Space Flight Center
Marshall Space Flight Center, Alabama

MSFC - Form 3190 (Rev June 1971)

TECHNICAL REPORT STANDARD TITLE PAGE

1. REPORT NO. NASA TM X-64890	2. GOVERNMENT ACCESSION NO.	3. RECIPIENT'S CATALOG NO.
4. TITLE AND SUBTITLE Status of Flow Separation Prediction in Liquid Propellant Rocket Nozzles		5. REPORT DATE November 1974
		6. PERFORMING ORGANIZATION CODE
7. AUTHOR(S) Robert H. Schmucker		8. PERFORMING ORGANIZATION REPORT #
9. PERFORMING ORGANIZATION NAME AND ADDRESS George C. Marshall Space Flight Center Marshall Space Flight Center, Alabama 35812		10. WORK UNIT NO.
		11. CONTRACT OR GRANT NO.
		13. TYPE OF REPORT & PERIOD COVERED Technical Memorandum
12. SPONSORING AGENCY NAME AND ADDRESS National Aeronautics and Space Administration Washington, D.C. 20546		
		14. SPONSORING AGENCY CODE

15. SUPPLEMENTARY NOTES

Prepared by Structures and Propulsion Laboratory, Science and Engineering

16. ABSTRACT

Flow separation plays an important role in the design of a rocket engine nozzle. For a given ambient pressure, the condition of "no flow separation" limits the area ratio and, therefore, the vacuum performance. Avoidance of performance loss due to area ratio limitation requires a correct prediction of the flow separation conditions. To provide a better understanding of the flow separation process, the principal behavior of flow separation in a supersonic overexpanded rocket nozzle is described. The hot firing separation tests from various sources are summarized, and the applicability and accuracy of the measurements are described. A comparison of the different data points allows an evaluation of the parameters that affect flow separation. The pertinent flow separation predicting methods, which are divided into theoretical and empirical correlations, are summarized and the numerical results are compared with the experimental points.

17. KEY WORDS	18. DISTRIBUTION STATEMENT Unclassified-unlimited A McCool A. A. McCOOL Director, Structures and Propulsion Laboratory

19. SECURITY CLASSIF. (of this report) Unclassified	20. SECURITY CLASSIF. (of this page) Unclassified	21. NO. OF PAGES 69	22. PRICE NTIS

MSFC - Form 3292 (Rev December 1972) For sale by National Technical Information Service, Springfield, Virginia 22151

ACKNOWLEDGMENTS

This research was performed under the NRC Resident Research Associateship program of the National Academy of Sciences at the Astronautics Laboratory, Propulsion and Thermodynamics Division (recently reorganized as the Structures and Propulsion Laboratory, Propulsion Division), NASA Marshall Space Flight Center (MSFC), Huntsville, Alabama. The encouragement given by C. R. Bailey, Scientific Advisor, K. W. Gross and H. G. Paul, Division Chief, during the tenure is highly appreciated.

TABLE OF CONTENTS

LIST OF ILLUSTRATIONS

LIST OF ILLUSTRATIONS (Concluded)

LIST OF TABLES

LIST OF SYMBOLS

Symbol	Definition
C_f	friction coefficient
F	thrust
H	form factor (δ^*/Θ)
I	momentum
k	constant
K	constant
m	mass flow rate
M	Mach number
p	pressure
r	radius
R_e	Reynolds number
T	temperature
u	velocity
w	wall condition
x	coordinate along the wall
y	coordinate normal to the wall
γ	isentropic exponent
δ	boundary layer thickness
δ^*	displacement thickness
e	natural logarithm base

Symbol	Definition
ϵ	area ratio
Θ_p	flow deflection angle
Θ_d	momentum thickness
Θ	nozzle wall angle
ρ	density
τ	shear stress

Subscripts

a	ambient
AS	Arens-Spiegler
c	combustion chamber
cha	characteristics
CL	Crocco-Lees
CP	Crocco-Probstein
DL	Donaldson-Lange
e	exit
e_b	boundary layer edge
f	friction
ff	full flow
i	initial point of separation region

LIST OF SYMBOLS (Concluded)

Subscripts	Definition
ic	incompressible
in	incipient
KB	Kalt-Bendall
M	Mager
nom	nominal
p	plateau
RTL	Reshotko-Tucker and Lawrence
s	separation
SCH	Schilling
t	throat
vac	vacuum
w	wall

TECHNICAL MEMORANDUM X-64890

STATUS OF FLOW SEPARATION PREDICTION IN LIQUID PROPELLANT ROCKET NOZZLES

INTRODUCTION

Flow separation occurs in an overexpanded supersonic rocket nozzle when the pressure at one point of the nozzle wall reaches a value which is 50 to 80 percent lower than ambient pressure. Such conditions exist when an engine designed for altitude operation is tested at lea level. This condition usually occurs during start transient, shut off transient, or engine throttling modes. Flow separation for steady state conditions is undesirable since the location of separation is unstable and leads to asymmetric and oscillating forces which can damage the nozzle and the engine mountings. Therefore, the area ratio for a nozzle under consideration is selected such that flow separation is not likely to occur. Prediction methods for determining the area ratio are based upon test data from hot firing and cold flow experiments, coupled with theoretical concepts. The performance optimization of an engine operating from sea level to vacuum conditions at a predetermined chamber pressure is controlled by two factors: (1) Both engine vacuum performance and weight increase with nozzle area ratio and (2) engine sea level performance and nozzle flow separation restrict area ratio increases. These conflicting requirements demand an accurately selected area ratio.

The first investigations concerning flow separation in nozzles were conducted by Buechner, Prandtl, Meyer, Fluegel and Stanton and were subsequently published by Stodola [1, 2, 3]. After World War II, this problem became increasingly important during the efforts in rocket engine design. The first well-known investigations of flow separation for hot fired nozzles were performed at the California Institute of Technology, by Forster and Cowles. Tests using a small nitric acid/aniline engine resulted in the separation correlation that wall pressures 60 percent below the ambient pressure produce flow separation. This quantity, sometimes called "Summerfield criterion [4]," was subsequently used for the design of nozzles and is still considered in many textbooks as a conservative rule [4, 5]. Since that time, much testing has been accomplished, especially with cold flow nozzles, and additional separation theories and correlations have been published. These have shown that the trend of the Caltech measurements was correct, but that the difference and the scatter of data at higher pressure ratios (chamber pressure divided by ambient pressure) becomes more pronounced. Due to the high chamber pressures and pressure ratios which are currently being used, the Summerfield criterion is not adequate to select the nozzle area ratio required to minimize flow separation but maximize engine performance.

The purpose of this report is to summarize all of the available hot firing separation data and to compare the results with existing theories. The effect of various significant parameters on flow separation is presented, providing an advanced approach to predict critical nozzle flow behavior.

THE PROCESS OF FLOW SEPARATION IN AN OVEREXPANDED NOZZLE

For the treatment of the flow separation process, a description of the various flow phenomena and associated definitions are necessary.

Description of the Principal Flow Separation Phenomenon

The flow field in an overexpanded rocket nozzle, with separation and corresponding wall pressure profile, is presented in Figure 1. Starting from the combustion chamber, the nozzle wall pressure can be predicted in the usual way by inviscid flow calculation using the method of characteristics[1]. Along the wall a boundary layer develops and grows in thickness as distance increases from the throat. Since the boundary layer of a rocket engine during hot firing is mostly turbulent, only turbulent separation will be considered. The pressure profile remains undisturbed downstream to the nozzle exit if the ambient pressure is negligible; this will be called vacuum pressure profile. When the ambient pressure p_a is higher than the exit wall pressure, a shock is required to compress the main flow to ambient conditions. The boundary layer can

1. The agreement between theoretical and experimental wall pressure is normally very good. The discrepancy of the wall pressure profiles for the J2-S engine [6] seems to be generated by measuring the mean between ambient and theoretical wall pressure due to slow responding transducer and long measurement lines.

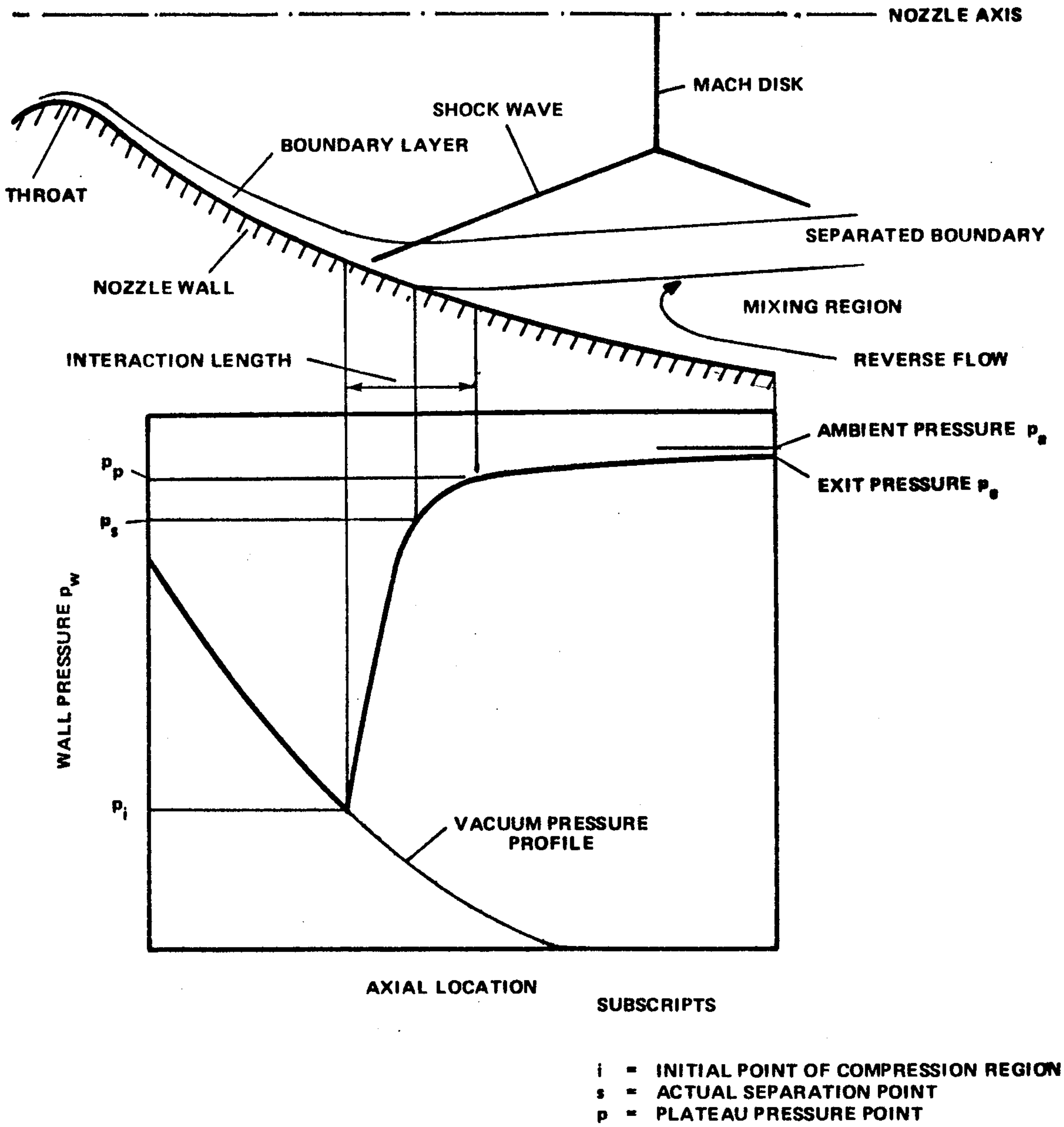

Figure 1. Flow field and pressure distribution in an overexpanded rocket nozzle with flow separation.

only withstand a certain pressure increase before the flow must separate from the wall. In this case, the flow expands normally in only one portion of the nozzle. At one point, always at the location where wall pressure is lower than ambient pressure, a sudden pressure rise is observed. In a very short distance, the wall pressure rises nearly to the ambient pressure. Due to this compression, the boundary layer thickens and an oblique shock wave is generated, which penetrates deep into the boundary layer. Within a few boundary layer thicknesses, the flow separates. The turning angle of the flow is rather constant, approximately 13.5 deg [7]. Downstream of the steep pressure gradient region, the wall pressure increases slowly to almost ambient pressure. The exit pressure p_e is generally slightly lower than the ambient pressure. Between the separated jet and the nozzle wall, the pressure difference recirculates the ambient air which mixes with the separated flow.

In this classical case of overexpanded supersonic nozzle flow separation, four different points and pressures can be defined:

1. i: The first deviation from the vacuum pressure profile occurs at point i; the compression of the flow starts here. This point is easily recognized since the pressure gradient of the separation region is very steep. It is important to remember that at i the flow has not yet separated.

2. s: The actual flow separation occures at point s. In cold flow tests this location is determined by oil film techniques, etc. However, since these methods are not applicable in hot firing tests, it is almost impossible to identify the exact point. The major pressure rise occurs in the region between i and s. Cold flow tests with forward facing steps, incident shocks, etc., indicate that more than 80 percent of the pressure rise occurs in this region [6]. The distance between i and s is small, approximately three boundary layer thicknesses according to data from wind tunnel tests. This differs from the data presented by L. H. Nave [8] for cold flow nozzles, in which only one boundary layer thickness between i and s is measured.

3. p: From point p, the pressure increase is rather small. According to the behavior of the pressure gradient, this point is sometimes called the "plateau pressure point." Its location is rather difficult to define since the pressure gradient between i and the nozzle exit does not vanish completely. In the region between i and p, the whole separation process occurs. This distance is called interaction length and covers a distance of approximately six boundary layer thicknesses. This value agrees well in different measurements [7, 8]. In Figure 1, it seems unlikely that 80 percent of the pressure rise is accomplished within the length equivalent to one boundary layer thickness.

4. e: In the region between p and the nozzle exit, the final pressure adjustment occurs. It is very small for normal configurations and is controlled by the nozzle geometry. The exit pressure is slightly lower than ambient pressure. Between p and e, a fairly linear pressure increase is measured. In some tests with contoured nozzles of low exit angle this pressure distribution seems to be different in character from the previously described one. Here the pressure gradient becomes steeper in the last portion of the nozzle than immediately downstream of the plateau point. This behavior seems to be only the result of plotting the pressure distribution as a function of area ratio rather than nozzle length, for example, since in a contoured nozzle the change of the area ratio is smaller with decreasing distance from the exit.

In general, no reattachment occurs after flow separation in rocket nozzles. During some tests with small cold and hot firing nozzles [8, 9, 10], a different pressure behavior and associated flow field has been experienced. As an example, one measurement of Stromsta [9] is presented in Figure 2. In this case, the gases expand in the nozzle to a lower wall pressure than would occur at pure separation. A rise in pressure exceeding the ambient pressure is observed in the separation region. Similar behavior occurs in ducts with supersonic flows [11]. The oblique shock wave emerging from the boundary layer is reflected by the Mach disk, which almost completely covers the nozzle cross section. Because of the reflection, the flow reattaches and the nozzle exit appears to flow full. The maximum pressure rise agrees approximately with that of a normal shock. The few available data indicate that this phenomenon can occur in small contoured nozzles with low exit angles. In these configurations, a normal shock can develop and lead to a pressure higher than ambient pressure. Furthermore, the boundary layer flow in small nozzles occupies a comparatively larger area than in large nozzles. No data, including those of transient wall pressure measurements, of this phenomenon are available for large nozzles. Separation and reattachment requires a lower chamber pressure for a full flowing nozzle than for pure separation. Therefore, the normal flow separation process can be considered as the upper limit and the separation-reattachment phenomenon will not be discussed.

Incipient Separation

With changing chamber pressure or ambient pressure, the separation region changes its position. The wall pressure distribution normalized with the chamber pressure is presented in Figure 3 for different chamber pressure

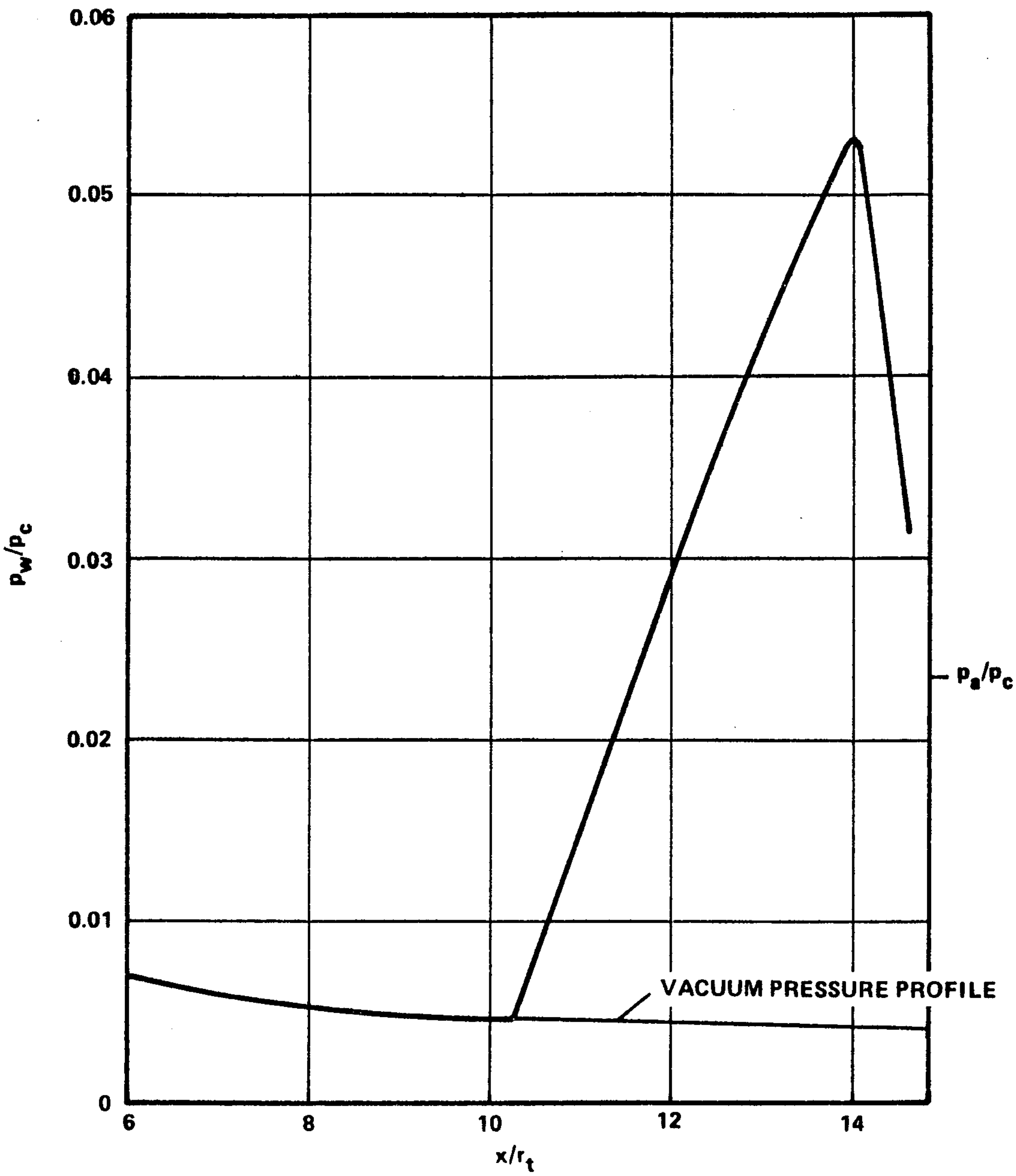

Figure 2. Separation and reattachment [9].

levels as a function of the axial distance from the throat normalized with the throat radius. Experience shows that the normalized wall pressure profile exhibits the same profile in the unseparated region, indicating a relatively negligible influence of the chamber pressure. At a chamber pressure which results in an exit wall pressure much lower than ambient pressure, the

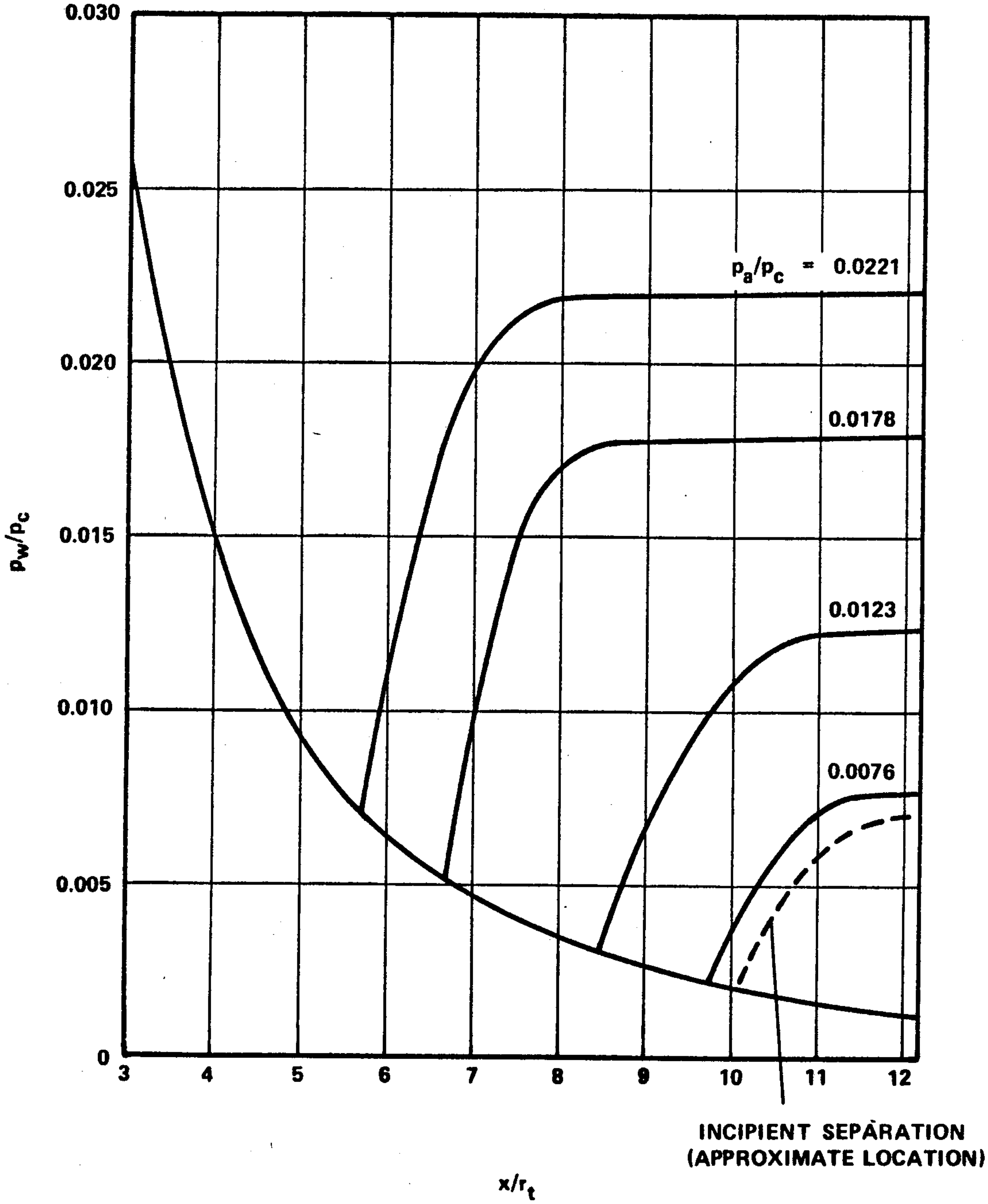

Figure 3. Wall pressure distribution as a function of axial location for different chamber pressures [13].

common separation pressure profile is established. An increase of the chamber pressure moves the separation region downstream. The mixing region becomes smaller while the interaction length of the separation region becomes larger since the boundary layer thickness grows along the wall. The position of the first pressure rise is a function of the pressure ratio p_c/p_a, and is presented in Figure 4. At a certain chamber pressure, the mixing region almost disappears and the interaction length ends with the nozzle exit. In this case, the plateau pressure agrees with the nozzle exit pressure. A further small increase of the chamber pressure moves the separation region partially out of the nozzle so that the complete interaction length cannot develop within the nozzle. In this case, the expression "flow separation" is no longer valid, since the flow is only compressed at the nozzle exit. Accurate wall pressure measurements show a pressure rise over a distance of a few boundary layer thicknesses. Since this pressure increase is similar to normal flow separation and, therefore, often mistaken as flow separation, the term "end effect" is sometimes used for this condition [8, 12].

The characteristic of pressure distribution with changing chamber pressure leads to the question: At which minimum condition does the nozzle flow full? This condition, also called "incipient separation," specifies the chamber pressure and wall pressure at which the flow separates exactly at the nozzle exit. Wall pressure measurements cannot identify the exact location of the separation point. The position of the first pressure rise point, p_i, as a function of the chamber pressure exhibits no characteristic behavior which could be connected with incipient separation. Therefore, it is reasonable to define incipient separation as the condition at which the interaction length ends at the nozzle exit.

The minimum wall pressure for incipient separation is obtained by pressure measurements like those in Figure 3. For every chamber pressure, a minimum wall pressure exists in Figure 3; in the case of flow separation, this is the pressure p_i. If only compression at the nozzle exit occurs (end effect), a minimum wall pressure also is observed and is lower than ambient pressure. Plotting these minimum nozzle wall pressures as functions of chamber pressures results in a graph similar to Figure 5. With increasing chamber pressure the minimum wall pressure decreases. When the separation region is close to the nozzle exit, the pressure p_i reaches a minimum range. Up to this chamber pressure, the flow always separates within the nozzle. An increase of the chamber pressure raises the minimum wall pressure and results in an oblique shock at the exit. Finally, when the chamber pressure is high enough, the exit pressure and the ambient pressure agree. During this region of chamber pressure increase, the nozzle always operates at overexpanded conditions.

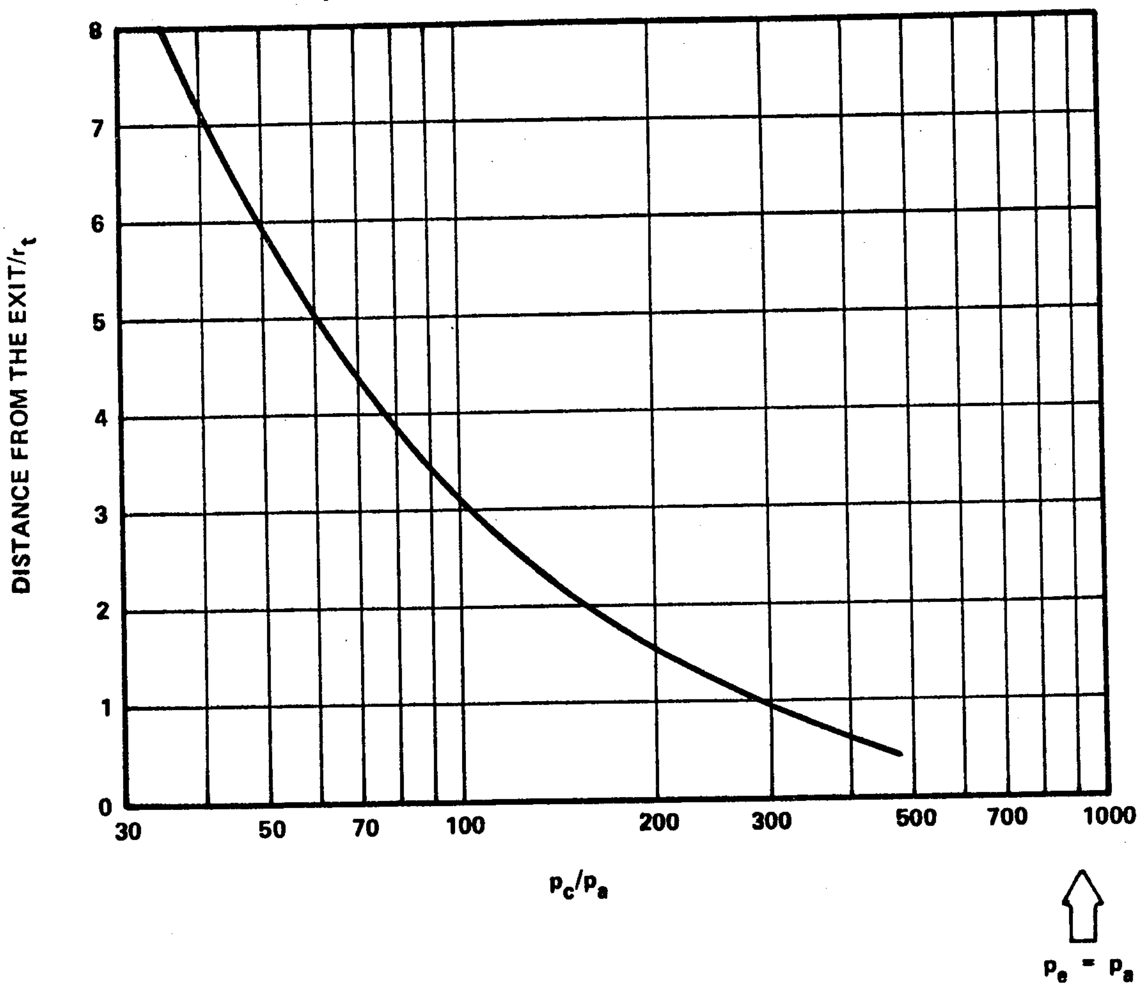

Figure 4. Distance of the first pressure rise point i from the nozzle exit as function of the pressure ratio [13].

The wall pressure at point p_i as a function of the chamber pressure in Figure 5 shows a rather flat minimum. This pressure corresponds to the previously defined condition of incipient separation, thus one can measure the incipient separation wall pressure. Since the minimum of Figure 5 covers a certain range of chamber pressures, it is reasonable to use the upper limit for the incipient separation chamber pressure.

One minimum wall pressure belongs to every chamber pressure in Figure 5. During experiments, a hysteresis effect has been noted which leads to a small region of different wall pressures, especially at incipient separation and reattachment. The value of the minimum wall pressure depends on the direction of the chamber pressure change. When the chamber pressure of a full flowing nozzle is lowered, incipient separation occurs at a lower wall pressure, as compared with the incipient separation wall pressure when the chamber pressure is raised to move flow separation out of the nozzle [8, 12]. A general statement about the width of this hysteresis band is not possible at the present time.

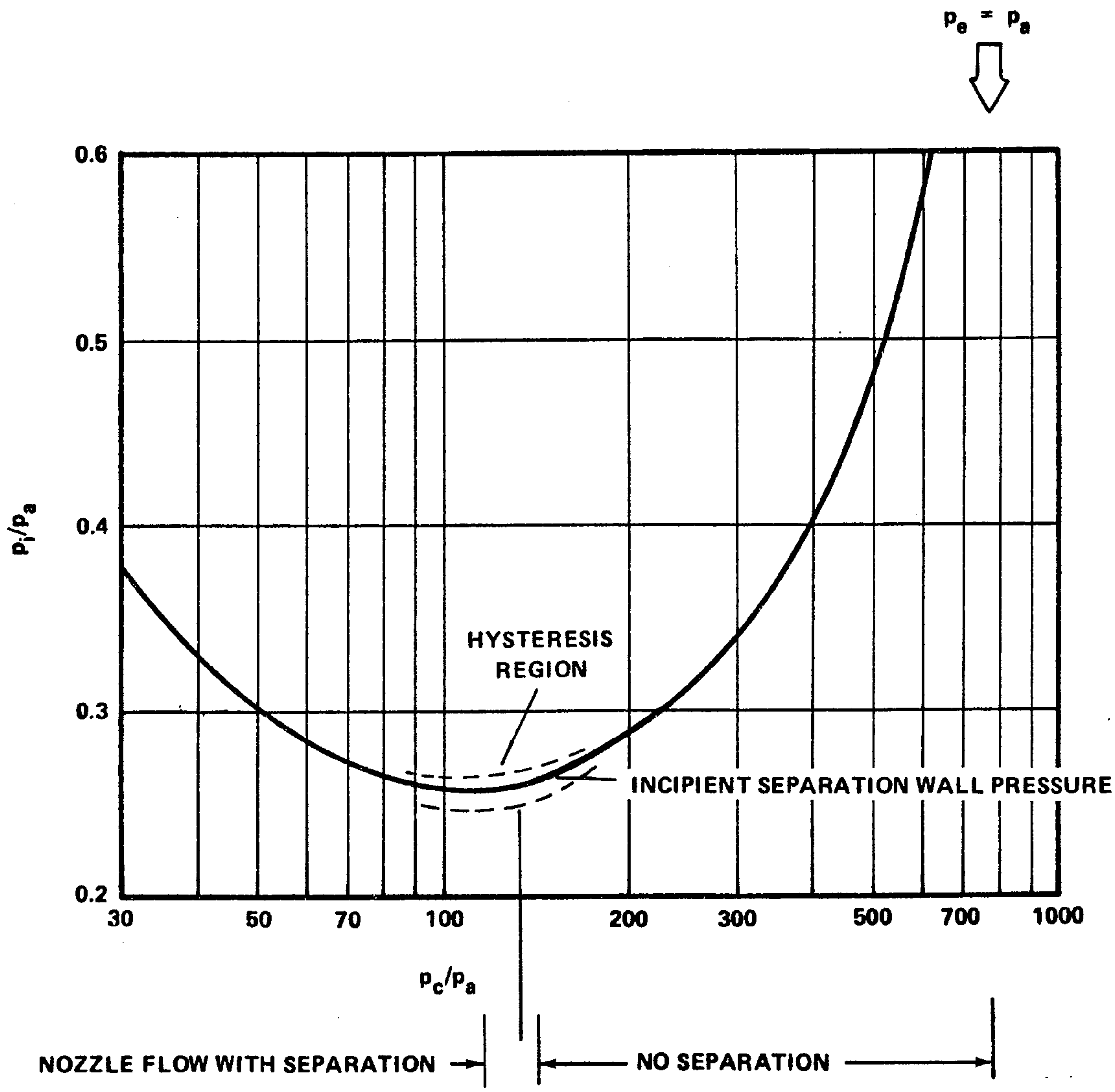

Figure 5. Minimum nozzle wall pressure as function of chamber pressure [13].

Separation Criterion

The basic criterion for design of a nozzle operation at fixed ambient conditions is the minimum value of the vacuum profile exit pressure $p_{e_{vac}}$ required to obtain a full flowing nozzle. Since this pressure depends on the ambient pressure, a normalization with the ambient pressure is necessary and the ratio which describes the condition for full flow is

$$p_{e_{vac}}/p_a \geq K_{ff} \quad . \tag{1}$$

where K_{ff} is a function of nozzle parameters. With a known K_{ff} and a given ambient pressure, the nozzle area ratio must be selected so that the corresponding exit pressure from the vacuum pressure profile divided by the ambient pressure is greater than K_{ff}.

For incipient separation, the wall pressure reaches a minimum value $p_{i_{in}}$ and, according to equation (1), a ratio is defined which describes the condition of incipient separation:

$$p_{i_{in}}/p_a = K_{in} \quad . \tag{2}$$

$$\approx p_i/p_p \quad . \tag{2a}$$

The condition of incipient separation is the limiting case for a full flowing nozzle, requiring the equivalence of K_{ff} and K_{in} for this condition:

$$K_{in} = K_{ff} \quad . \tag{3}$$

This relation is only an approximation. For a positive nozzle pressure gradient, the pressure $p_{i_{in}}$ is always higher than $p_{e_{vac}}$. Therefore, equation (3) results in reliable values for the wall pressure and equation (1) can be rewritten as

$$p_{e_{vac}}/p_a \geq K_{in} \quad . \tag{4}$$

K_{in} must be obtained from experiments or advanced analyses.

EXPERIMENTAL RESULTS

For the design of the nozzle area ratio, the factor K_{in} must be known. This can be done by measuring the separation conditions of similar engines and scaling the results to the required condition. This leads to some questions such as: How similar must the tested nozzles be and what scaling laws have to be applied? This question may be expressed in another way: What are the main influential factors on nozzle flow separation and how do they affect the separation condition? One way to answer this question is to compare the results of flow separation measurements in different engines under various conditions.

Flow Separation Measurements

By measuring the minimum wall pressure as a function of chamber pressure, the value of K_{in} for one configuration can be established. However, most of the available separation data specify only the separation pressure ratio p_i/p_a for one chamber pressure. However, the pressure increase in the mixing region for normal nozzle configurations is small and the results of these separation measurements do not deviate too much from those of incipient separation. Therefore all the available separation measurements of hot firing nozzles can be used for the establishment of the experimental results.

Experimental Data. Experimental data are available from many sources. These sources and the important engine parameters are summarized in Table 1. The flow separation measurements are listed in the Appendix.

Some comments are necessary about some of the measurements. Although the data of Forster and Cowles [14] from Jet Propulsion Laboratory (JPL) and Boomer et al. [13] from NASA-Lewis Research Center are rather old, they are still one of the most extensive measurements over a wide range of engine parameters. The accuracy of these is as good as recent data. The data of Sunnley and Ferriman from Bristol-Siddley are not too accurate, since the data had to be evaluated from the diagrams of Reference 12 and the RL-10 measurements are somewhat questionable. In these tests and in some of the J-2 and J-2S measurements, cyrogenic cooling of the wall caused freezing of the transducer lines. Therefore, the condition "no side loads" together with the theoretical wall pressure was used as an upper limit for full flow. Some transient wall pressure measurements are available from NASA-MSFC tests. The pressures were obtained by using the position of the first pressure rise point and the theoretical wall pressure since the transient wall pressures are not very reliable. Experimental and theoretical wall pressures agreed very well during steady state. The Pratt & Whitney Aircraft Division data of a high pressure engine are the result of short duration tests of 0.5 to 1 sec. Closeup high speed motion pictures [15] indicated that the nozzles were flowing full. In some of the measurements made by Thayer and Booz from Pratt & Whitney Aircraft using small models of the Space Shuttle Main Engine (SSME) baseline, booster and orbiter nozzle separation and reattachment occurred. These data deviate very much from the rest of the data, so these results should not be used for evaluation of pure separation.

Plotting Method. The primary consideration for the evaluation of experimental data is the selection of a plotting method. There are many methods for the graphical representation but some of them may not emphasize the most important information. In the case of flow separation, this problem is not yet solved. Two methods are widely used: (1) plotting the separation pressure ratio as a function of Mach number at point p_i and (2) using various pressure ratios.

In many flow separation theories, the Mach number at point p_i is the most important parameter. Ahead of the separation region, the momentum of the boundary layer must withstand the pressure differential to ambient pressure. Since the momentum change of the velocity profile in the separation region and the pressure increase are related, an expression of the form

TABLE 1. SOURCES OF HOT FIRING SEPARATION DATA AND ENGINE DESCRIPTION

Symbol	Source	Propellants	$p_{c\,nom}$ [a] (N/cm^2)	F_{nom} [b] (N)	ϵ [c]	Θ [d] (deg)	W [e]	T [f]	Remarks
○	Forster and Cowles (JPL) [14]	HNO_3/aniline	200	3300	10	15	s	c	(γ = 1.23)
					20	15			
					10	10			
					10	20			
					10	30			
□	Bloomer et al (NASA-Lewis RC) [13]	O_2/kerosene	220	13000	50	20	s	c	(γ = 1.24)
					42	25			
					75	25			
					60	30			
□	Sunnley and Ferriman [12]	H_2O_2/kerosene	370	22000	10	17	t	c	(γ = 1.20)
□	(Bristol-Siddley)		370	89000	14	17	t	c	
◇	Atlas Sustainer (Rocketdyne) [37]	O_2/kerosene	400	270000	25	15	t	c	(γ = 1.24)
⬡	J-2S engine (Rocketdyne) [7]	O_2/H_2	820	1200000	40	b	t	cc	no side loads (γ = 1.26)
⬡	J-2 engine (Rocketdyne)	O_2/H_2	450	1000000	27	b	t	cc	no side loads (γ = 1.26)
⬡									transient data
▽	J-2 model engine (Rocketdyne)	O_2/H_2	450		27	b	s	c	
⬭	RL-10 engine (Pratt & Whitney) [38]	O_2/H_2	200	67000	60	b	t	cc	freezing in sense lines
▷	Kah and Lewis (Pratt & Whitney) [15, 39]	O_2/H_2	2040	44000	250	b	s	u	short duration tests
					205				
					125				
▷					100				
					99				
◁	Thayer and Booz [10]	O_2/H_2	340	900	35	b	s	c	
◁	(Pratt & Whitney Aircraft)				35	b	s	c	
					80	b	s	c	
△	NASA-MSFC 4k-engine	O_2/H_2	680	1800	20	18°	s	u	

a. $p_{c\,nom}$ — design chamber pressure
b. F_{nom} — design thrust
c. ϵ — expansion ratio
d. Θ — nozzle angle (b for bell nozzle)
e. W — wall surface: s smooth wall, t tube wall
f. T — wall temperature: u uncooled, c cooled, cc cryogenically cooled

$$p_p - p_i = f_i\left(\rho_i/2\, u_i^2\right) - f_p\left(\rho_p/2\, u_p^2\right) \tag{5}$$

can be assumed. The values u_i, ρ_i, u_p, and ρ_p are the velocity and density of the gases at the boundary layer edge at points i and p, respectively. Expressing the flow properties at point p by the properties at point i using isentropic core flow or oblique shock flow relations, then rearranging with the velocity of sound and dividing by p_i yields:

$$p_p/p_i = g_1\left(M_i^2\,\gamma/2\right) \quad , \tag{6}$$

or with $p_p \approx p_a$,

$$p_i/p_a = g_2\,(M_i) \quad . \tag{7}$$

According to equation (7) the separation criterion is a function of Mach number at the first pressure rise point.

The method of plotting pressure ratios started with Summerfield's p_i/p_a versus p_c/p_a [3]. This method showed a large scatter of the data, especially at higher chamber pressures. Therefore, Green used $(p_a - p_i)/p_c$ instead of p_i/p_a and achieved a suppression of the scatter, but this was merely due to the larger scale of the diagram [1]. Finally, Schilling used p_i/p_c versus p_c/p_a [16]. Again, the big scatter of the Summerfield plotting method disappeared, but more or less due to the larger scale. A further discussion of this method will be presented in the next section.

According to these results, the method p_i/p_a versus M_i will be used for principal representation of the experimental results.

Accuracy of the Separation Measurements. The accuracy of experimental data is always limited by measurement errors. Since the wall pressure is measured by only a limited number of transducers, the exact location of the first deviation from the vacuum pressure profile cannot be accurately defined. As an example, the separation measurements obtained with a 4K lox/H_2 engine at NASA/MSFC will be discussed. In Figure 6, the wall pressure distribution of different tests is plotted. The wall pressures for unseparated conditions agree well, but there is small scatter which might be affected by the accuracy of the transducers, voltage input, surface and measurement hole irregularities, etc. In the case of separation, the wall pressure shows good agreement with the previous tests down to the separation region. Between the stations at approximately 21.5 and 23 cm distance from the throat, the pressure rise occurs. The transducer at 23 cm indicates a time dependent behavior. According to the wall pressure scatter and the limited number of transducers, the envelope is presented within which the real pressure distribution should be included. From the pressure distribution at the different station, it seems more likely that the point p_i is little downstream of the station at 21.5 cm. This leads to a maximum scatter for the pressure at point p_i of 0.2 N/cm^2, about 6 percent of the absolute value. This possible error must be introduced in the evaluation of this experimental point.

This indicates that all experimental data for the determination of the separation condition have a scattering range of about 5 to 10 percent. In some of the available test data, due to the few transducers, this possible error may be greatly exceeded. Therefore all pressure data of point p_i must be used with some caution, and the accuracy should be considered if some conclusions about "obvious" effects are to be drawn.

Summary of Hot Firing Separation Data

The plotting of separation data in the Appendix requires the calculation of the Mach number M_i and point p_i. The core flow is normally considered to be isentropic. Therefore,

$$M_i = \left\{ \frac{2}{\gamma-1} \left[\left(\frac{p_c}{p_i} \right)^{\frac{\gamma-1}{\gamma}} - 1 \right] \right\}^{0.5} \tag{8}$$

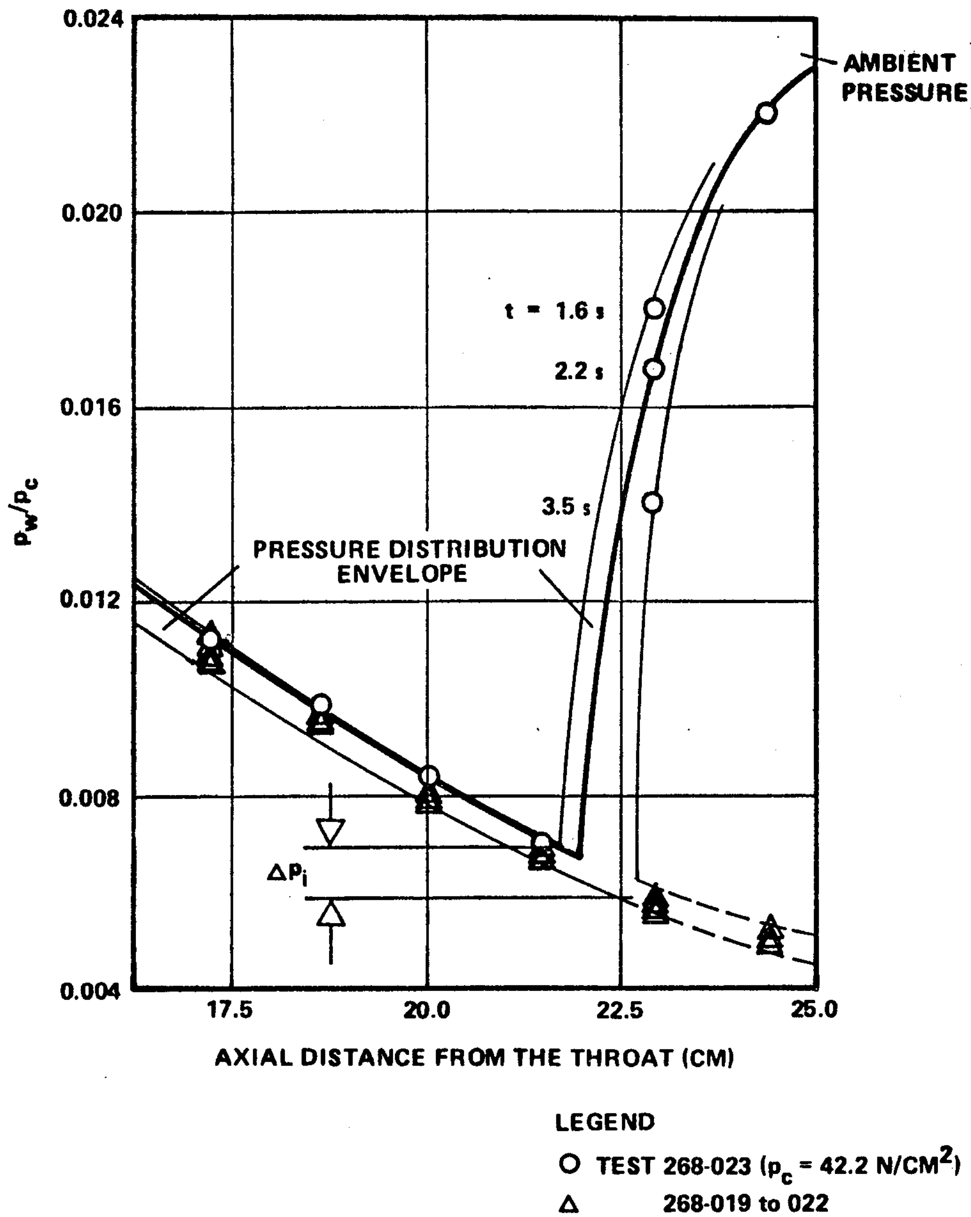

Figure 6. NASA-MSFC 4K engine separation tests (lox/H_2).

can be used [5, 6]. Equation (8) is based on a constant isentropic exponent during the expansion. Although the isentropic exponent for real combustion products changes during the expansion, equation (8) describes the local Mach number very well. Small deviations of the mean isentropic exponent do not affect the calculated Mach number significantly. The isentropic exponents of the various propellant combinations are listed in Table 1 [5, 6, 17].

The hot firing data of the Appendix are presented in Figure 7. As additional information, an envelope of the available cold flow data obtained from References 18, 19, 20, and 21 and summarized in Reference 8 is also shown. The shaded field represents the majority of the cold flow data.

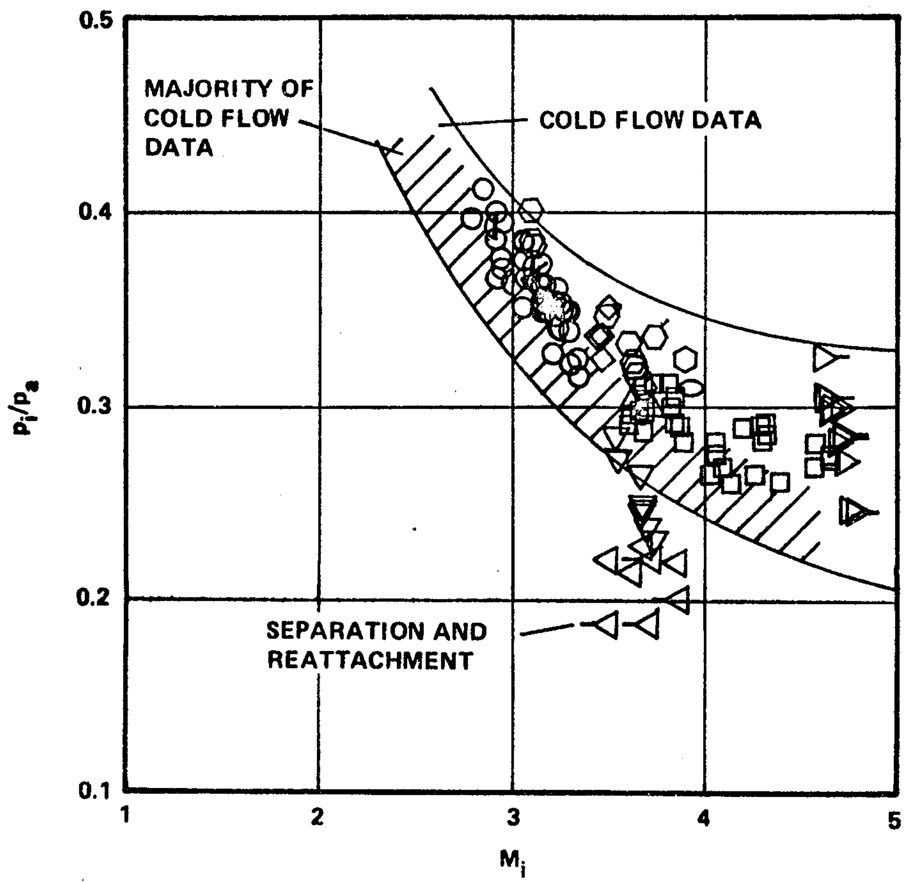

Figure 7. Hot firing separation data (see Table 1 for symbols).

The data points of Figure 7 indicate that the general trend of cold flow and hot firing experiments agrees. With increasing Mach number at the first pressure rise point, the separation pressure ratio decreases. The cold flow envelope also covers the hot firing data points, but the majority of the cold flow separation pressure ratios is 10 to 15 percent lower than the hot firing data. (It is possible that the upper envelope of the cold flow data does not represent a true separation condition. These data might be "end effect" conditions.) The results of two hot firing experiments with small contoured nozzles do not agree with this analysis. These are the separation measurements with a J-2 model and three SSME model nozzles. The separation pressure ratios are much lower than the rest of the data. In some of these tests, especially in Reference 10, separation and reattachment occurred. The hot firing data will be discussed in more detail. For an investigation of the influence of the different parameters on flow separation, a reduction of the scatter is necessary to clarify the diagram. It was stated previously that all measurement scatters were at least 5 to 10 percent. A common method for reduction of measurement errors is the averaging of several experimental data, which were obtained under the same general conditions. Using the previous test data and averaging the measurements of each engine, within certain Mach number limits, will result in the diagram presented in Figure 8.

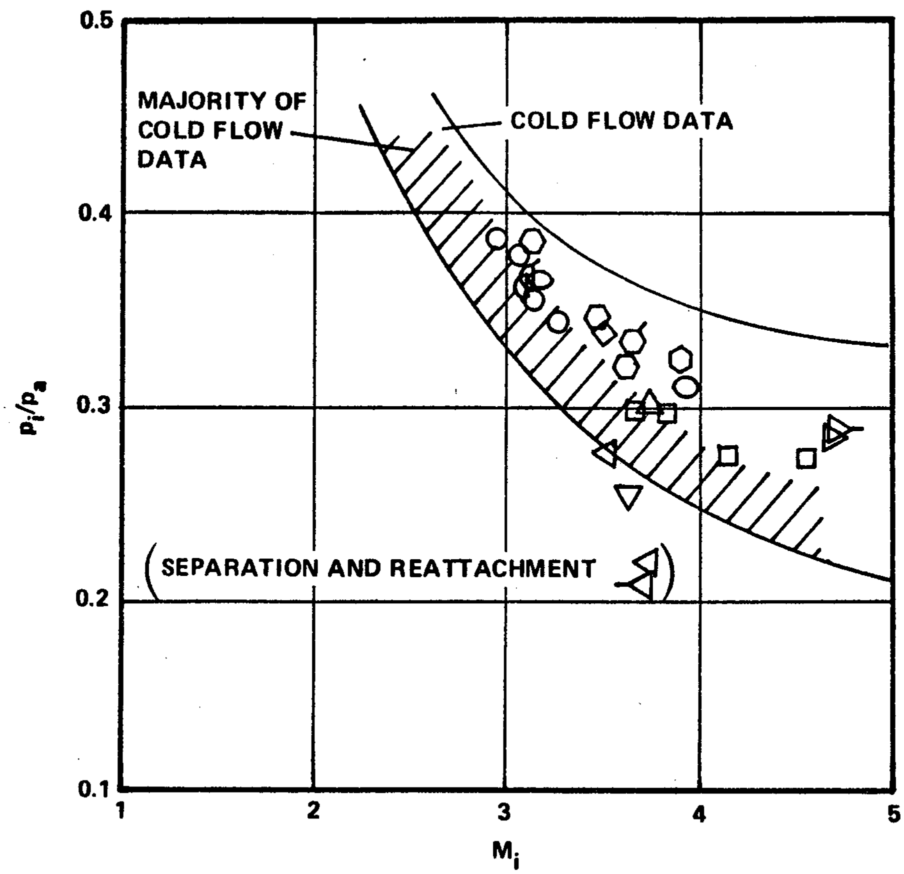

Figure 8. Averaged hot firing separation data as function of M_i (see Table 1 for symbols).

The big scatter of Figure 7 almost completely disappears. The hot firing data are located at the upper limit of the majority of the cold flow data. A large discrepancy between these cold flow data and hot firing data exists, especially at higher Mach numbers. The experimental data of small contoured nozzles, in which no reattachment was observed, agree with the lower limit of the cold flow data. The tests with reattachment show a much lower separation pressure ratio.

Influence of Various Parameters on Separation Condition

The averaged separation data of hot firing nozzles from Figure 8 will be used for investigation of the influence of various parameters on the separation condition.

With increasing Mach number ahead of the separation region, the separation pressure ratio decreases. At higher Mach numbers, the Mach number dependence becomes small and the separation pressure ratio probably does not go beyond a certain limit, which is greater than zero. This tendency is similar for the cold flow data. Some unpublished data of separation tests with gaseous hydrogen, which are graphically represented in Reference 22, result in a separation pressure ratio of 0.2 at a Mach number of 6.2, indicating that the limit probably lies between 0 and 0.1 for cold flow tests. In the case of hot firing nozzles, according to the data points of Figure 8, this limit might be higher.

The separation pressure ratio for different cone angles is presented in Figure 9. The available data cover angles from 10 to 30 deg. The data points obtained at a Mach number of approximately 3 indicate that the 10 deg nozzle separates later (this means a lower separation pressure ratio) than the 20 deg nozzle. The 15 deg nozzle agrees with this trend, but the 30 deg nozzle data points lie between that of the 10 and 20 deg nozzle. The data at a Mach number of 4 do not show any trend with the cone angle. This leads to the conclusion that the angle effect on the separation pressure ratio is either nonexistent or very small. For a separation prediction this effect must be neglected.

The change of the separation pressure ratio with different engine sizes is presented in Figure 10. The distinction of the three engine sizes — small, medium and large — is somewhat arbitrary. Comparing the different data points and using the majority of the cold flow data from Figure 8, which are normally for small nozzles, indicates that there is a small trend related to engine size. Such a statement must be used with caution since the data of the large engines are not as reliable as the data of medium and small engines. The "no side load" points of the large J-2 and J-2S engines, especially, result in a too high separation pressure ratio. Since a scatter of the experimental data still exists and a falsification of the trend by other effects such as nozzle contour, etc., is possible, the only probable conclusion is that the separation pressure ratio is either independent of the engine size or increases little with engine size.

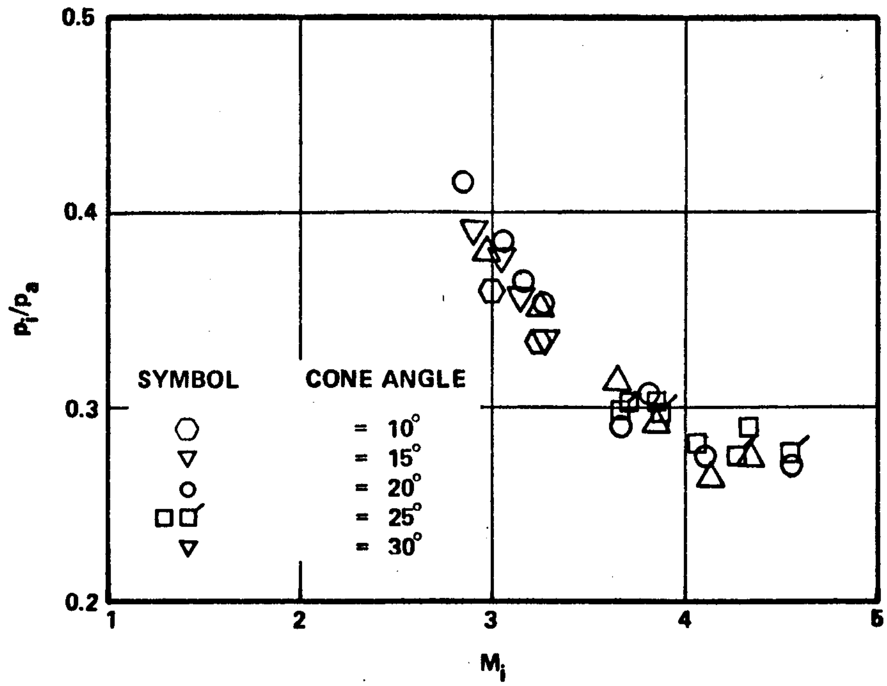

Figure 9. Effect of the cone angle on the separation pressure ratio.

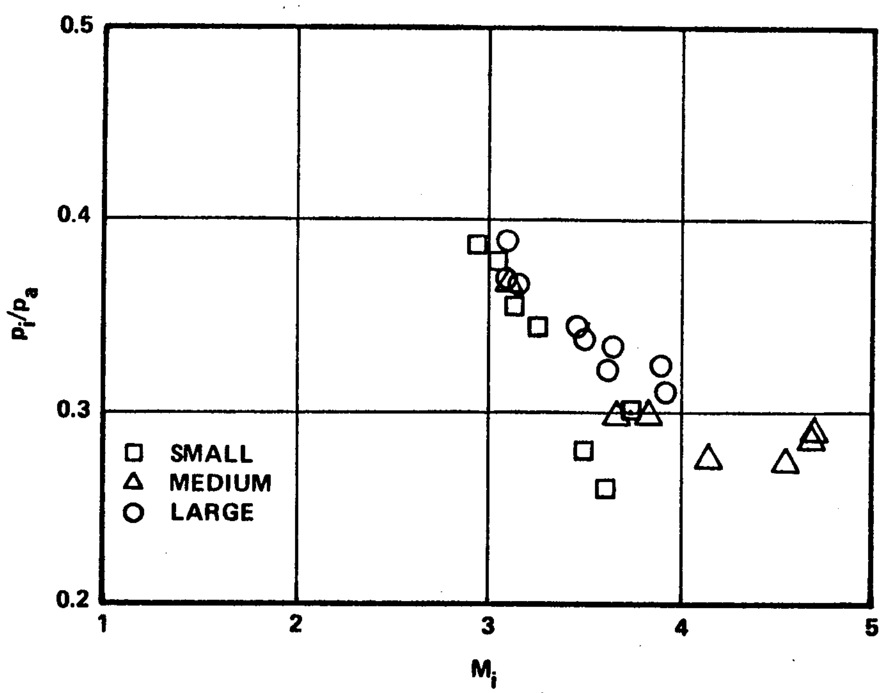

Figure 10. Effect of the engine size on the separation criterion.

The influence of the nozzle configuration — conical or contoured — on the separation pressure ratio is presented in Figure 11. The separation pressure ratio of the contoured nozzles is little higher than that of the conical nozzles. This difference is so small that no obvious discrepancy between conical and contoured nozzles can be stated. This is in contrast to some previously published statements that contoured nozzles separate later than conical nozzles, but these results normally were obtained from small cold flow nozzles.

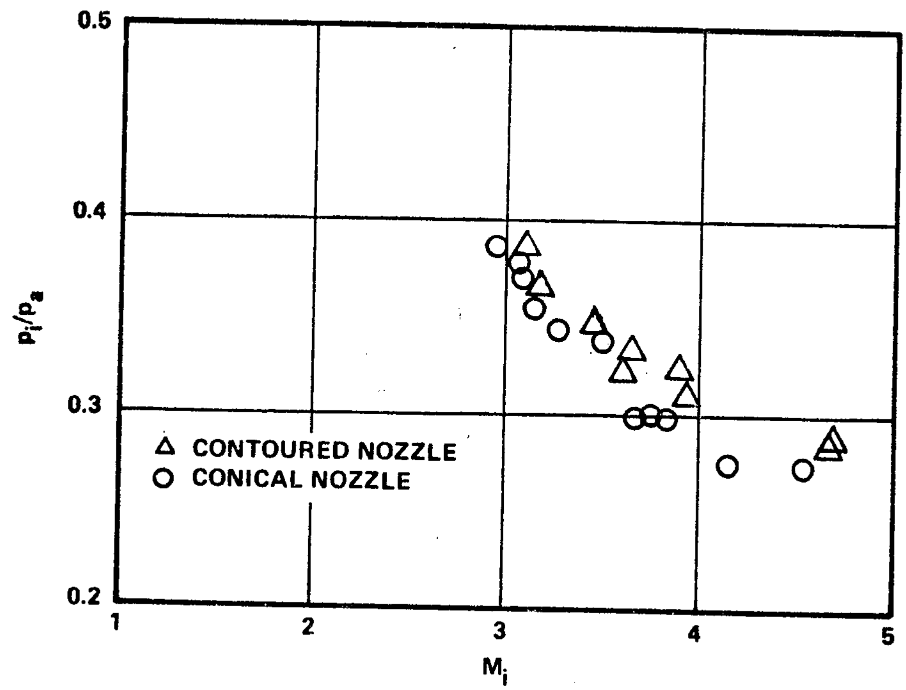

Figure 11. Change of the separation pressure ratio with nozzle configuration.

A difference of the separation behavior between nozzles with smooth and tube walls is supposed in Reference 8. The separation pressure ratio for these two wall configurations is presented in Figure 12. From the available data, it is obvious that the wall configuration has nearly no effect.

The influence of the wall temperature on the separation pressure ratio is shown in Figure 13. The difference of data points is so small that no effect of the wall temperature can be deduced. Even cryogenically cooled nozzles deviate only slightly from the uncooled and normally cooled walls. This seems to be in contrast to theoretical considerations of the wall temperature effect, since a cooler wall is normally believed to lead to a lower separation pressure ratio.

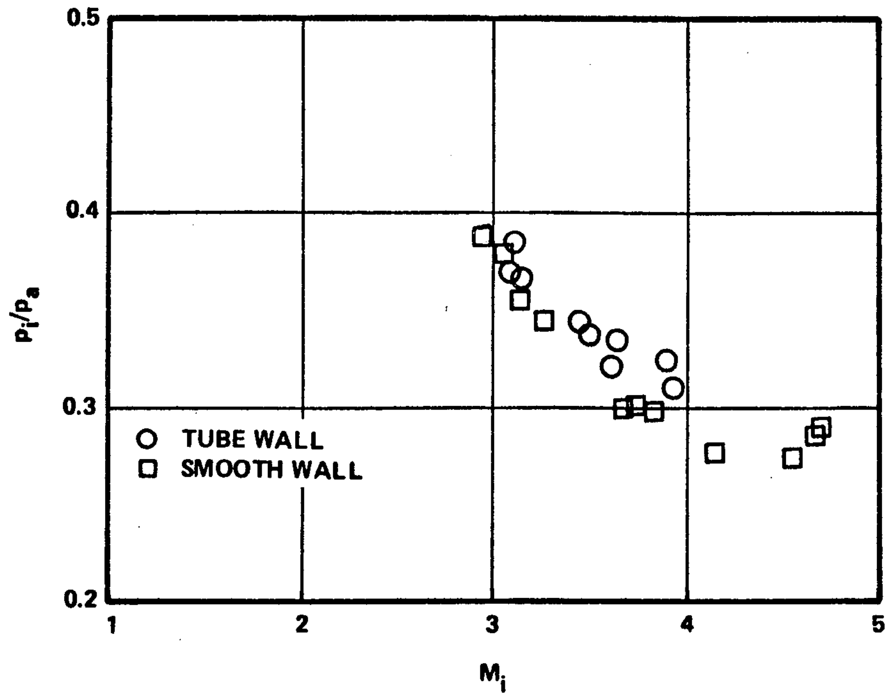

Figure 12. Wall configuration effect on the separation behavior.

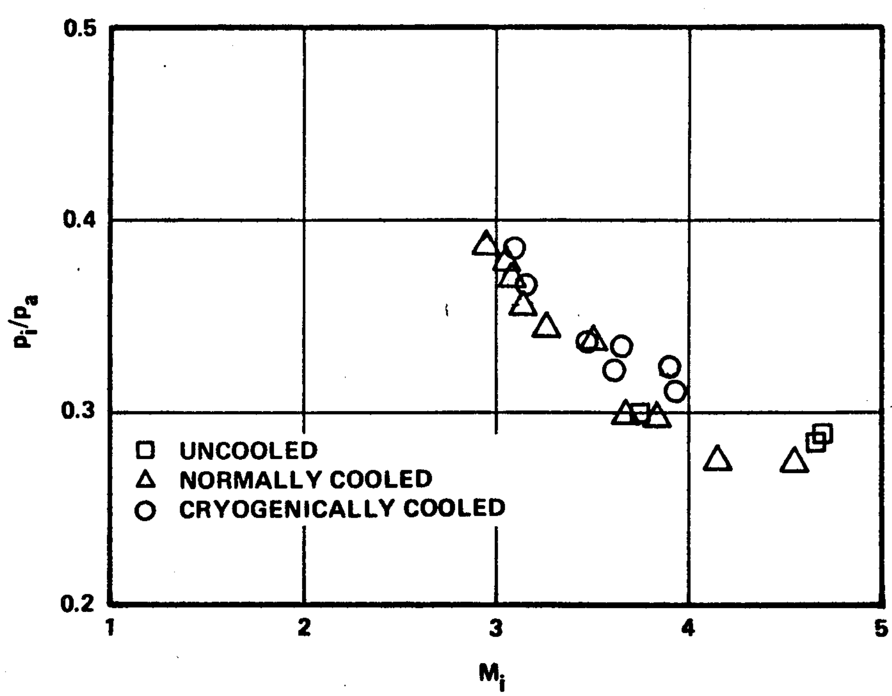

Figure 13. Cooling effect on the separation pressure ratio.

With the change of propellant combination, the isentropic exponent is altered. The effect of γ on the separation behavior is presented in Figure 14. No general trend is obvious so a negligible effect must be stated.

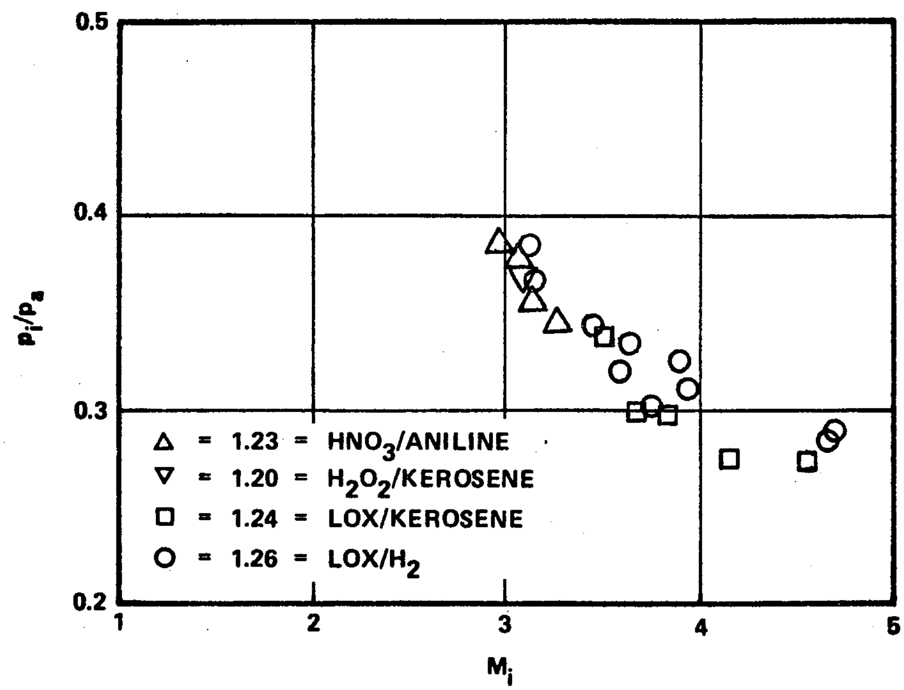

Figure 14. Change of the separation behavior for different isentropic exponents (propellant combinations).

Summary of Hot Firing Separation Results

The description of the separation behavior in a supersonic nozzle and the investigation of the effect of different parameters on the separation condition yielded the following conclusions about the present status of experimental flow separation research in hot firing nozzles:

1. The separation process occurs in a distance of a few boundary layer thicknesses.

2. Cold flow tests normally deviate from the hot firing results, probably due to size and contour effect.

3. Small contoured hot firing nozzles have a lower separation pressure ratio.

4. There is no difference between medium and large, conical and contoured nozzles.

5. Separation and reattachment decreases the separation pressure ratio.

6. The end effect pressure is not real separation condition.

The separation criterion K_{in} of hot firing nozzles shows the following trends:

1. With increasing Mach number ahead of the separation region, the separation criterion decreases.

2. A lower limit of the separation criterion probably exists.

3. K_{in} is not or only slightly affected by:

   a. Nozzle wall angle.

   b. Engine size.

   c. Nozzle contour.

   d. Wall configuration.

   e. Wall temperature.

   f. Propellant combination (isentropic exponent).

FLOW SEPARATION PREDICTION METHODS

Many flow separation prediction methods have been published. They can be divided into two groups, the theoretical methods and the empirical correlations. Most of them have their origin in high speed aerodynamics and were later applied to nozzle flow separation.

Flow Separation Theories

All of the theoretical flow separation predicting methods depend on empirical constants to fit the experimental results. In this section, these methods are summarized and their applicability is derived by comparing the theoretical results with the experimental findings. Although some of the theories are quite old they are still in use for rocket nozzle flow separation prediction.

Donaldson-Lange [23]. Donaldson and Lange derived one of the first theories for flow separation [11]. It is assumed that the pressure rise is governed by the shear forces in the separation region. The analysis predicts the plateau pressure rise at a flat plate.

The separation shock wave penetrates deep into the boundary layer. In the region near the wall, at a distance $k_{DL_1}\delta$, where δ denotes the boundary layer thickness and k_{DL_1} a proportionality factor, the shock wave is spread over a small distance, the length of which is $k_{DL_2}\delta$, where k_{DL_2} is again a proportionality factor. Separation will occur when the momentum change by the shear force is equal to the momentum change by the pressure rise. Assuming that the net amount of momentum that remains in the element $k_{DL_1}\delta \cdot k_{DL_2}\delta$ is proportional to the initial shear stress τ_i, the proportionality is

$$(p_p - p_i)\, k_{DL_1}\, \delta \sim \tau_i\, k_{DL_2}\, \delta \quad , \tag{9}$$

or after dropping the proportionality factors and dividing by the density and velocity of the flow at the boundary layer edge at point p_i,

$$\frac{\dfrac{p_p}{p_i} - 1}{p_i \dfrac{\rho i}{2} u_i^2} \sim \frac{\tau_i}{\dfrac{\rho_i}{2} u_i^2} \quad . \tag{10}$$

The right-hand term of equation (10) represents the skin friction coefficient. For a turbulent flow over a flat plate with a one-seventh power law, the friction coefficient depends on the length Reynolds number Re_x

$$C_f = \frac{\tau_i}{\frac{\rho_i}{2} u_i^2} \tag{11}$$

$$\sim Re_x^{-0.2} \quad . \tag{12}$$

Introducing equation (12) into equation (10) and expressing the velocity and density by the Mach number and the isentropic exponent of the gases yields

$$\frac{p_i}{p_p} = \frac{1}{1 + M_i^2 \frac{\gamma}{2} k_{DL_3} Re_x^{-0.2}} \tag{13}$$

$$= K_{in_{DL}} \quad . \tag{13a}$$

The factor k_{DL} must be evaluated from experiments. Equation (13) predicts a strong Reynolds number dependence of the separation pressure ratio. With increasing Re_x, the separation criterion decreases.

Although the experimental data seem to indicate a small trend of the separation pressure ratio with engine size, the 0.2 power of the length Reynolds number is too high. Presently, there is general agreement that the plateau pressure rise is independent or only slightly dependent on the Reynolds number [24]. It was stated by R. Lange [23] that equation (13) does not describe the experimental trend. Equation (13) should, therefore, not be used for separation pressure ratio predictions [24].

The "obvious" agreement between theory and experiment in Reference 23 is the result of changing Reynolds number and Mach number simultaneously in the tests so that the Mach number dependence was incorrectly explained by the Reynolds number.

Mager [25, 26]. Mager was the first to use an expression of the form

$$\frac{M_s}{M_i} = k_M \quad , \tag{14}$$

where k_M is a constant. Dividing the total pressure rise into the pressure rise before and after the separation point results in

$$\frac{p_i}{p_p} = \frac{p_i}{p_s} \frac{p_s}{p_p} \quad . \tag{15}$$

Using an approximation for the oblique shock relation, the pressure rise from p_i to p_s can be written as

$$\frac{p_i}{p_s} = \frac{1}{1 + \frac{\gamma}{2} M_i^2 \frac{1 - k_M}{1 + \frac{\gamma - 1}{2} M_i^2}} \quad . \tag{16}$$

Downstream of the separation point, the flow turns its direction and the momentum change results in a pressure increase. With a Stewartson transformation of the compressible boundary layer equations to the incompressible form, this pressure ratio can be expressed by

$$\frac{p_p}{p_s} = 1 + 0.328 \frac{\gamma M_s^2 \Theta_p}{1 + \frac{\gamma - 1}{2} M_s^2} \quad . \tag{17}$$

As Θ_p describes the final turning angle of the separated jet, the factor 0.328 results from the transformation and the form factors of a separated boundary layer. Combining equations (14) through (17) yields

$$\frac{p_i}{p_a} = \frac{1}{1 + \frac{\gamma}{2} M_i^2 \dfrac{1 - k_M}{1 + \frac{\gamma - 1}{2} M_i^2}} \quad \frac{1}{1 + 0.328 \dfrac{\gamma M_i^2 k_M^2 \Theta_p}{1 + \frac{\gamma - 1}{2} M_i^2 k_M^2}} \tag{18}$$

$$= K_{in_M} \quad . \tag{18a}$$

An iterative solution of equation (18) is necessary since the turning angle depends on the Mach number M_i and the pressure ratio.

The result of equation (18) and the experimental data points are presented in Figure 15. Although the trend of the Mach number effect is right, the absolute numbers disagree with the experimental points. Some comments about Mager's correlation in References 6 and 27 point out that the deviation from the experimental data at higher Mach numbers is caused by the linearized approximation of the oblique shock equation in equation (16). No improvement of equation (16) of Mager's original approach has been made. The modification by Gruman [28] does not change the result significantly.

Obviously Mager's relation does not describe the actual flow separation process accurately enough. Therefore Mager's flow separation criterion, equation (18), should not be used for separation predictions.

Reshotko-Tucker [27] and Lawrence [1, 29]. Similar to Mager's Mach number ratio method, Reshotko and Tucker and, subsequently, Lawrence derived an equation resulting in a Mach number ratio before and after the separation region, utilizing some experimental boundary layer values of incompressible flow separation. Although no distinction between the points p_s and p_p is made, the results can also be applied for the plateau pressure rise.

Assuming a constant pressure across the boundary layer and neglecting the shear forces in the separation region, Karman's integral momentum

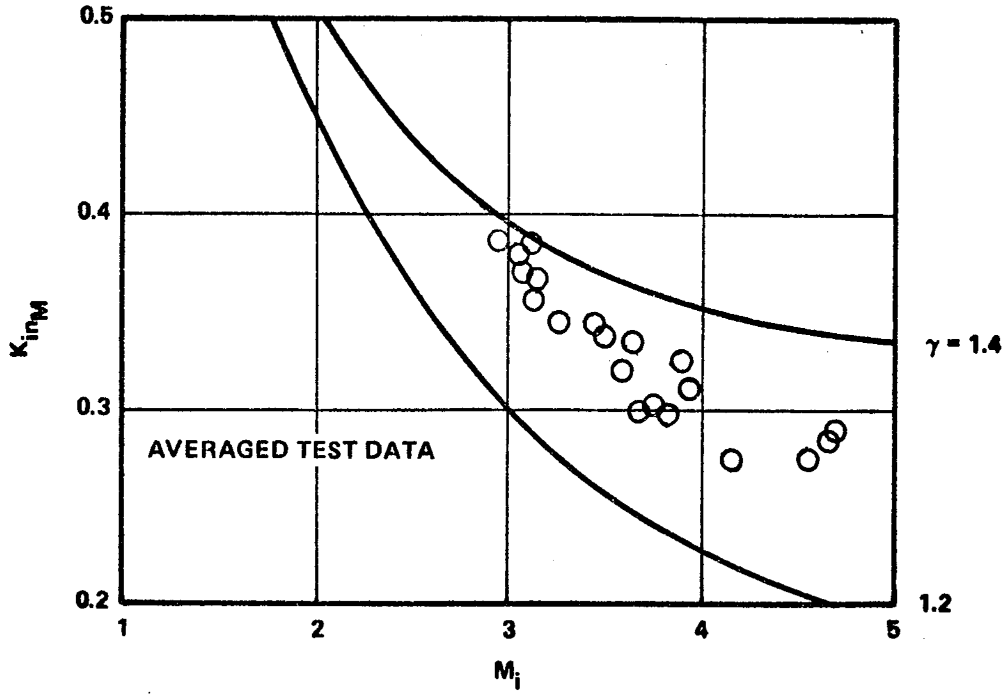

Figure 15. Mager's separation criterion ($K_M = 0.55$).

equation can be written as

$$\frac{dI}{dx} - u_e \frac{d\dot{m}}{dx} + \delta \frac{dp}{dx} = 0 \quad , \tag{19}$$

where I and $\dot{m}$ indicate the momentum and mass flow rate. The boundary layer nomenclature is shown in Figure 16. The components I and $\dot{m}$ may be expressed by the boundary layer thickness δ, the displacement thickness δ^*, the momentum thickness Θ_d, and the shape factor H. Using the following definitions:

$$\delta^* = \int_0^\delta \left(1 - \frac{\rho u}{\rho_{e_b} u_{e_b}}\right) dy \quad , \tag{20}$$

$$\Theta_d = \int_0^\delta \frac{\rho u}{\rho_{e_b} u_{e_b}} \left(1 - \frac{u}{u_{e_b}}\right) dy \quad , \tag{21}$$

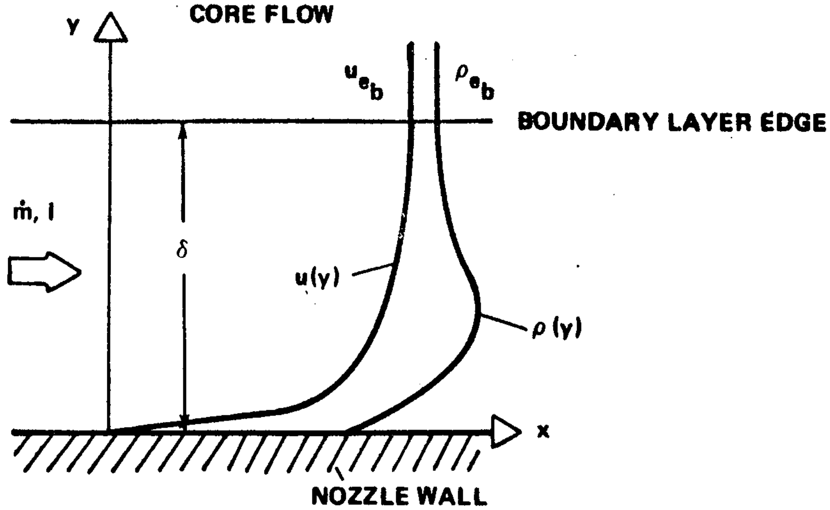

Figure 16. Definitions of the boundary layer flow.

and

$$H = \frac{\delta^*}{\Theta_d} \quad , \tag{22}$$

the mass flow rate and momentum are

$$m = \rho_{e_b} u_{e_b} \delta \left(1 - \frac{\delta^*}{\delta}\right) \quad , \tag{23}$$

and

$$I = \rho_{e_b} u_{e_b}^2 \delta \left[1 - \frac{\delta^*}{\delta} \left(1 + \frac{1}{H}\right)\right] \quad . \tag{24}$$

From equation (19), the moment-of-momentum equation is obtained by multiplying the integrand of the momentum integral equation by the distance y, normal to the surface, and integrating with respect to y. Using a modified Stewartson transformation to transform the compressible boundary layer equation to the same form as the incompressible equation and integrating the moment-of-momentum equation leads to a relation between the Mach number and the form factor. With H_{ic} as incompressible form factor according to equations (20) through (22), the expression is

$$M = \frac{\left(H_{ic}^{2}\right) e^{[1/(H_{ic}+1)]}}{\left(H_{ic}^{2}-1\right)^{0.5}\left(H_{ic}+1\right)} k_{RTL_1} \tag{25}$$

$$= M\left(H_{ic}\right) \quad . \tag{25a}$$

The proportionality constant of equation (25) is eliminated by using the Mach number ratio across the separation region

$$\frac{M_{p'}}{M_i} = \frac{M\left(H_{ic_p}\right)}{M\left(H_{ic_i}\right)} \quad , \tag{26}$$

or

$$\frac{M_p}{M_i} = k_{RTL} \quad . \tag{27}$$

This Mach number ratio can be used for the calculation of the pressure ratio across an oblique shock and one obtains

$$\frac{p_p}{p_i} = \frac{-M_i^2(\gamma+1)\left(k_{RTL}^2-1\right)}{2k_{RTL}^2 M_i^2(\gamma-1)+4}$$

$$+ \frac{\left\{M_i^4(\gamma+1)^2\left(k_{RTL}^2-1\right)^2+4\left[k_{RTL}M_i^2(\gamma-1)+2\right]\left[M_i^2(\gamma-1)+2\right]\right\}^{0.5}}{2k_{RTL}^2 M_i^2(\gamma-1)+4} \tag{28}$$

$$= 1/K_{in_{RTL}} \quad . \tag{28a}$$

The values of the form factor for equation (25) are obtained from experimental incompressible flow separation data. Along a flat plate with a one-seventh power velocity profile, the shape factor is $H_{ic_i} = 1.286$. In the case of separation, the form factor ranges from $1.8 < H_{ic_p}$ to 2.6. With an average value of 2.2 for H_{ic_p}, the Mach number ratio $k_{RTL} = 0.762$.

In Figure 17, this separation criterion is presented with $k_{RTL} = 0.762$ for different values of γ. The value $\gamma = 1.4$ results in a fairly good agreement with hot firing separation data, although all the data points have isentropic exponents in the range of 1.2 to 1.26. A reduction of the isentropic exponent to 1.2 leads to a big change of the separation criterion and a strong deviation from the experimental points. Such an effect has not been observed in the tests. This tendency is similar to Mager's γ effect and typical for most of the separation theories.

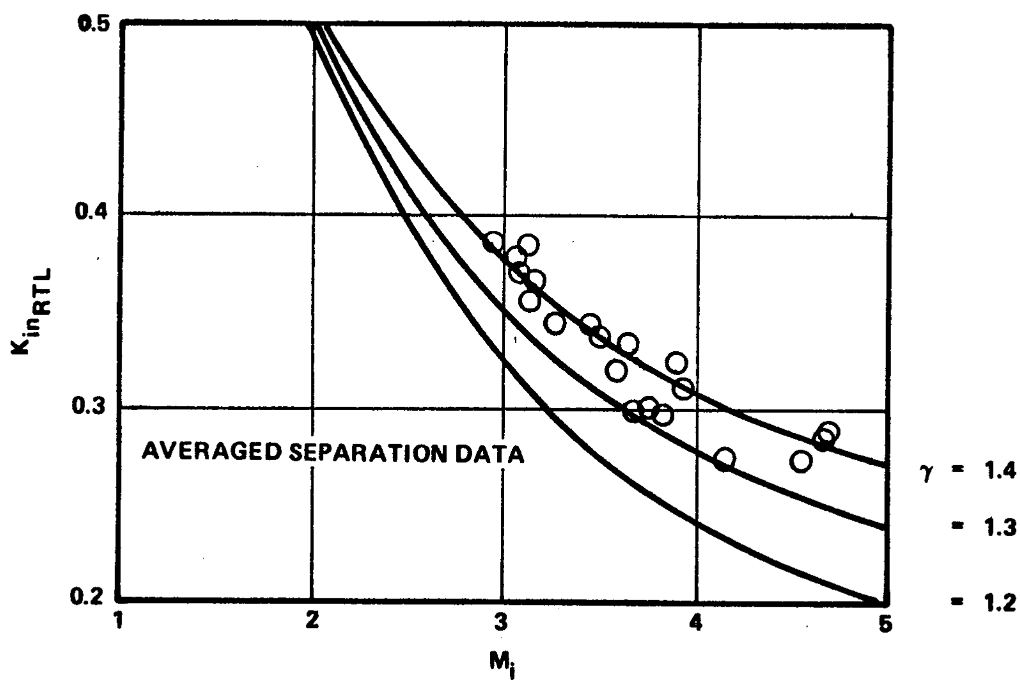

Figure 17. Reshotko-Tucker's separation criterion ($K_{RTL} = 0.762$).

Crocco-Probstein [30]. Crocco and Probstein developed one of the more sophisticated theories of the flow separation process. The model to be adopted is shown in Figure 18. The external flow is sharply deflected at the point where the shock wave emerges from the boundary layer. At the separation point, the usual boundary layer pressure predictions are not accurate; however, at a short distance upstream and downstream from this point the boundary layer calculations are valid. Therefore at points p_i and p_p, a constant pressure across the boundary layer can be assumed. Since the distance between p_i and p_p is only a few boundary layer thicknesses, the mass inflow and the skin friction can be neglected, allowing for the use of equation (19). Then, the continuity and momentum equation yields

$$\dot{m}_i = \dot{m}_p \tag{29}$$

and

$$I_i - I_p = \delta_i (p_p - p_i) \quad , \tag{30}$$

where $\dot{m}$ and I are obtained by equations (23) and (24). The change of the properties of the core flow across the shock wave is described by the Hugeniot-Rankine equation

$$\frac{T_p}{T_i} = \frac{\dfrac{\gamma + 1}{\gamma - 1} + \dfrac{p_p}{p_i}}{\dfrac{\gamma + 1}{\gamma - 1} + \dfrac{p_i}{p_p}} \tag{31}$$

where T is temperature.

Transforming the boundary layer equations with a Stewartson transformation from the compressible form to the incompressible form, according to the Crocco-Lees mixing theory [31], allows the definition of various

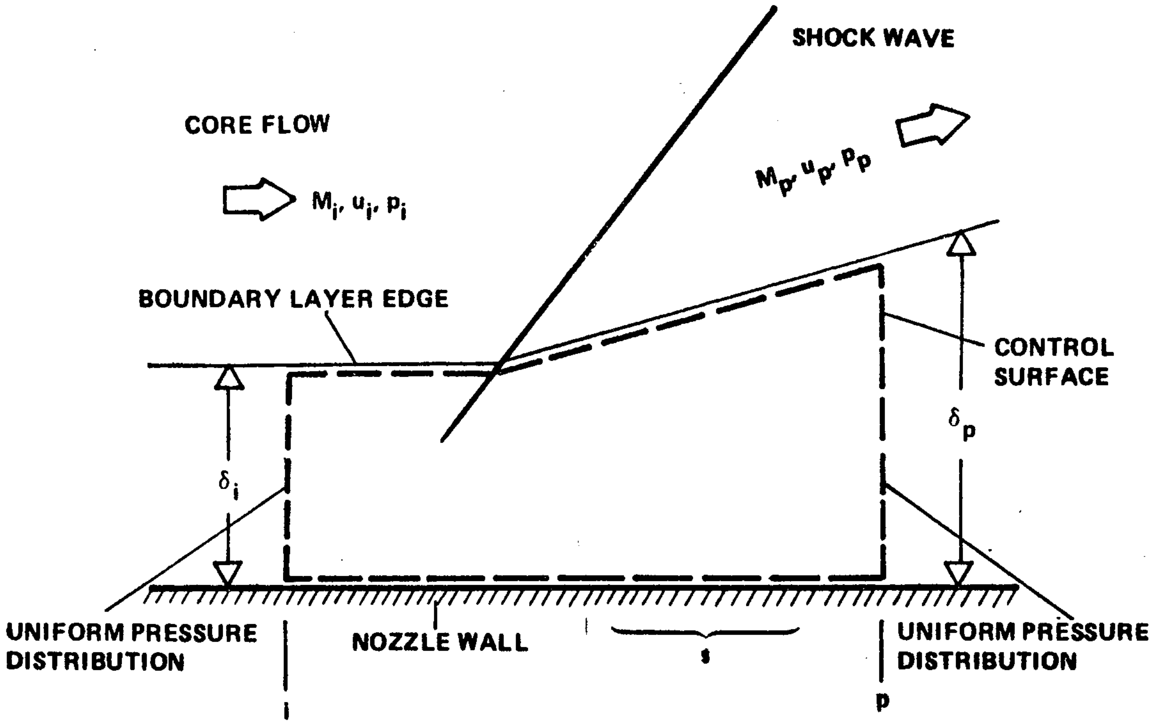

Figure 18. Crocco-Probstein's boundary layer model.

quantities:

$$k_{CL_1} = \left(\frac{1}{1 - \frac{\delta^*}{\delta} - \frac{\Theta_d}{\delta}} \right)_{ic} \tag{32}$$

and

$$k_{CL2} = \left(\frac{1 - \frac{\delta^*}{\delta} - \frac{\Theta_d}{\delta}}{1 - \frac{\delta^*}{\delta}} \right)_{ic} \quad , \tag{33}$$

where the velocity thickness, displacement thickness, and momentum thickness are those of the transformed incompressible boundary layer. Combining the transformed equations with the shock relation results in

$$\frac{p_p - p_i}{\gamma p_i}\left[k_{CL1_i}\frac{1}{M_i^2} + \frac{\gamma - 1}{2}\left(k_{CL1_i} - 1\right)\right]$$

$$= 1 - \frac{k_{CL2_p}}{k_{CL2_i}}\left(\frac{2}{\gamma - 1}\right)^{0.5}\frac{1}{M_i}\left(1 + \frac{\gamma - 1}{2}M_i^2 - \frac{\dfrac{\gamma + 1}{\gamma - 1} + \dfrac{p_p}{p_i}}{\dfrac{\gamma + 1}{\gamma - 1} - \dfrac{p_i}{p_p}}\right)^{0.5} \quad . \quad . \qquad (34)$$

For a given Mach number at station p_i, the pressure rise depends only upon the boundary layer value upstream and downstream of the separation region. Equation (34) can be solved for the Mach number and one obtains

$$M_i = \left\{\frac{K_{CP_2} + K_{CP_1}K_{CP_3} + \left[K_{CP_2}\left(K_{CP_2} + 2K_{CP_1}K_{CP_3}\right) + \left(\dfrac{K_{CL2_p}}{K_{CL2_i}}\right)^2 K_{CP_3}\right]^{0.5}}{2\left[K_{CP_1}^2 - \left(\dfrac{K_{CL2_p}}{K_{CL2_i}}\right)^2\right]}\right\}^{0.5}$$

(35)

with

$$k_{CP_1} = 1 - \frac{\gamma - 1}{2\gamma}\left(\frac{p_p}{p_i} - 1\right)\left(k_{CL1_i} - 1\right) \quad , \qquad (36a)$$

$$k_{CP_2} = \frac{2}{\gamma - 1}\left(\frac{k_{CL2_p}}{k_{CL2_i}}\right)^2 \frac{\frac{p_i}{p_p} - \frac{p_p}{p_i}}{\frac{\gamma + 1}{\gamma - 1} + \frac{p_i}{p_p}} , \tag{36b}$$

and

$$k_{CP_3} = \frac{2}{\gamma} k_{CL1_i}\left(\frac{p_p}{p_i} - 1\right) . \tag{36c}$$

The results for equations (35) and (36) are presented in Figure 19. The chosen values for k_{CL} indicate a good agreement with the experimental data. The effect of the isentropic exponent on the separation criterion is very small, which is in accordance with the experimental results. At higher Mach numbers, the reduction of the separation criterion with increasing Mach number almost disappears and the lower limit for K_{in}, with the boundary layer values used, lies between 0.12 and 0.19.

Since this separation theory not only results in an agreement with theoretical and experimental data but also exhibits the same trend of Mach number and γ effect, it is usable for flow separation prediction. The small γ influence allows a rather arbitrary selection of γ without significantly changing the result.

Arens-Spiegler [32, 33]. Arens and Spiegler's approach is based on the suggestion of Gadd [34] that the pressure rise required to separate a turbulent boundary layer is obtained by using the assumption that pressure rise must be sufficient to stagnate a characteristic velocity in the boundary layer. With the ratio of the characteristic velocity u_{cha} to the boundary layer edge velocity $u_{e_{b_i}}$, the equation for the supersonic stream line is

$$k_{AS} = \frac{u_{cha}}{u_{e_{b_i}}} . \tag{37}$$

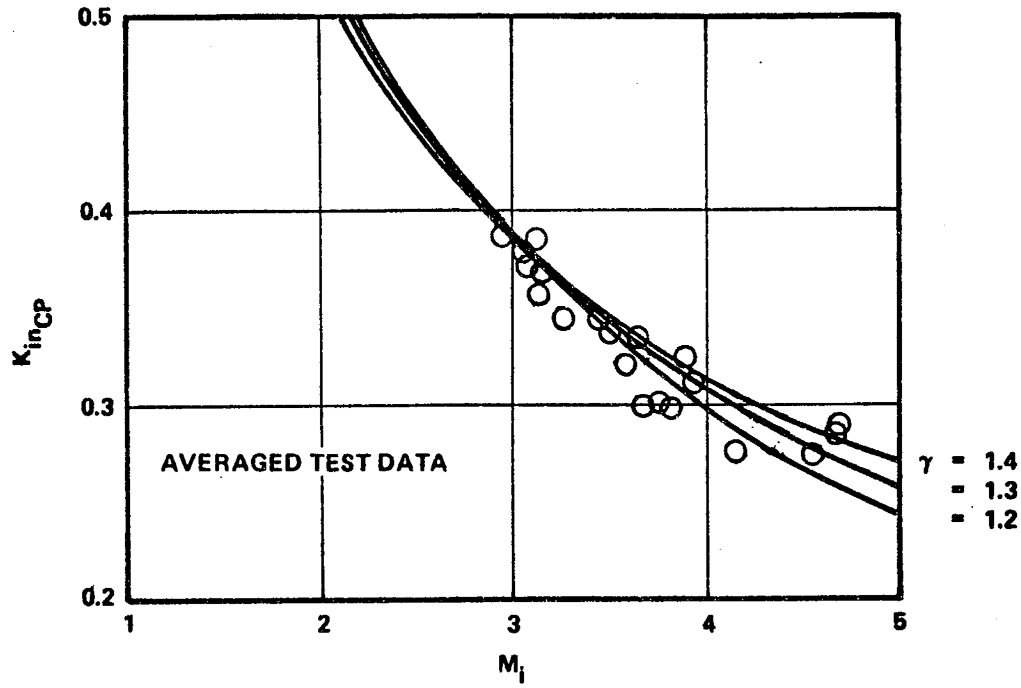

Figure 19. Crocco-Probstein's separation criterion $\left(K_{CL1_i} = 1.40,\ K_{CL2_p}/K_{CL2_i} = 0.865\right)$

The separation criterion is written as

$$\frac{p_i}{p_p} = \frac{\left[1 + \frac{\gamma - 1}{2} M_i^2 \left(1 - k_{AS}^2\right)\right] \left\{0.5 M_i^2 \left[(\gamma + 1) k_{AS}^2 - \frac{(\gamma - 1)^2}{\gamma + 1}\right] \frac{\gamma - 1}{\gamma + 1}\right\}^{\frac{1}{\gamma - 1}}}{\left(\frac{\gamma + 1}{2} M_i^2 k_{AS}^2\right)^{\frac{\gamma}{\gamma - 1}}}$$

$$= K_{in_{AS}} \quad . \tag{38}$$

This separation criterion and the averaged experimental data are presented in Figure 20. Good agreement is claimed in Reference 32, but only the general trend of the Mach number influence is right. The deviation with changing isentropic exponent is very strong and K_{in} decreases too rapidly with Mach number, especially at higher values of M_i. Since the experimental data

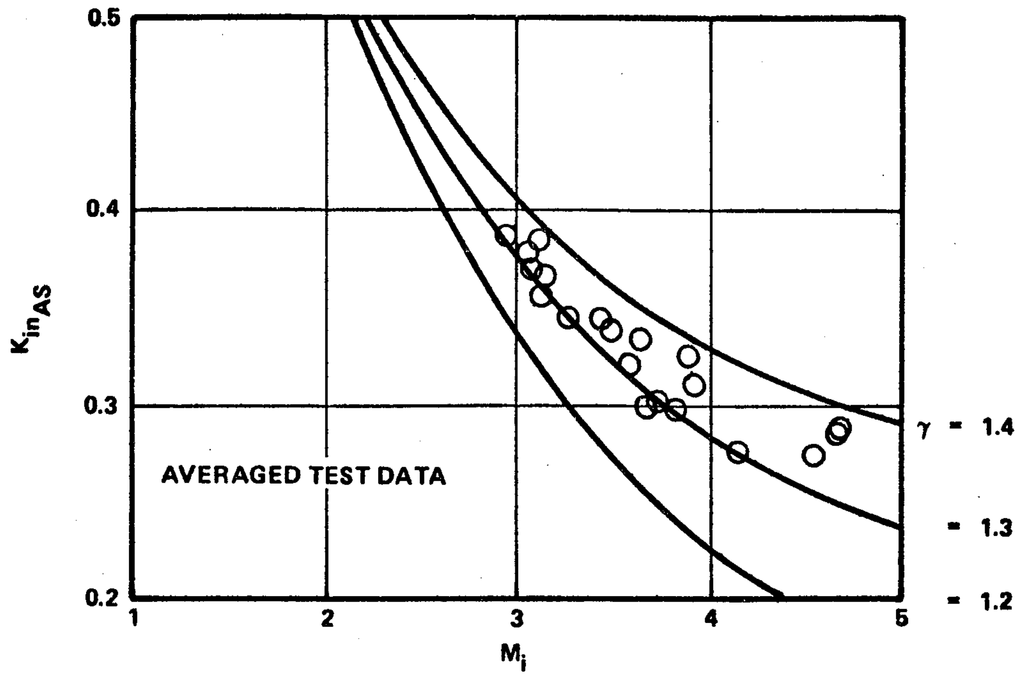

Figure 20. Arens-Spiegler's separation criterion ($K_{AS} = 0.60$).

do not show such a trend, k_{AS} seems to be a function of γ and M_i only in order to achieve a better fit to the data points. This leads to the conclusion that Arens and Spiegler's flow separation equation does not predict the real separation condition very well.

Empirical Flow Separation Prediction Methods

The empirical flow separation prediction equations are based on relations between certain pressure ratios rather than p_i/p_a versus Mach number. In Figure 21, the averaged separation points are graphically presented in the form p_c/p_i as a function of the chamber pressure ratio p_c/p_a. The test data are close together and it seems that this plotting method reduces the scatter of the experimental data. However, if in addition to the test points, the lines p_i/p_a = constant are used, it is obvious that only the scale of the p_i/p_a trend is reduced. Any change of the separation criterion is superimposed by the change of the chamber pressure ratio. Therefore, only the deviation from the 45 deg lines of Figure 21 are important for a separation criterion establishment.

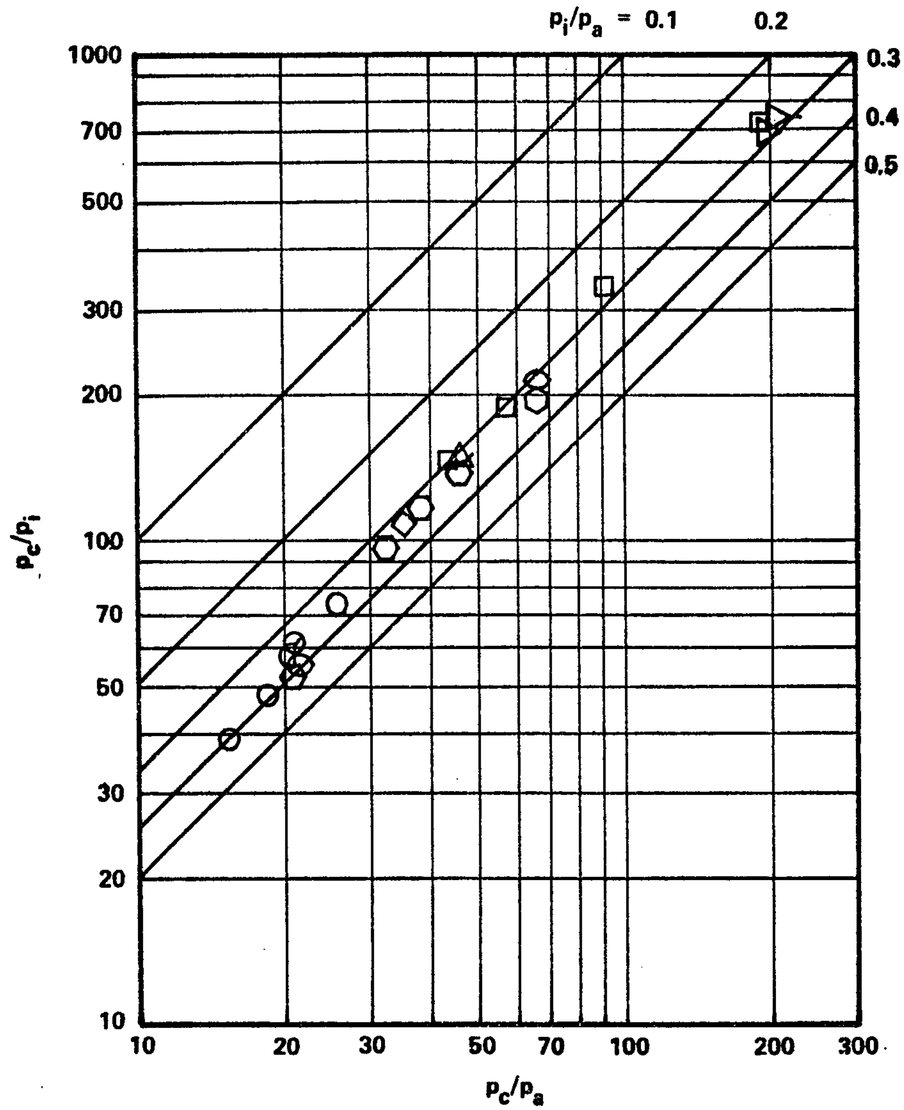

Figure 21. Averaged separation pressures as function of the chamber pressure ratio with lines of constant p_i/p_a (see Table 1 for symbols).

Schilling [16]. Schilling, quoted in Reference 32, proposed an equation of the form

$$p_i/p_c = k_{SCH_1} (p_c/p_a)^{k_{SCH_2}} . \tag{39}$$

Multiplying equation (39) with p_c/p_a yields

$$p_i/p_a = k_{SCH_1} (p_c/p_a)^{k_{SCH_2} + 1}$$

$$= K_{in_{SCH}} \quad . \tag{40}$$

The experimental data used by Schilling indicated short contoured nozzle constants of 0.583 and -1.195, respectively. Equation (39) with the previous constants is presented in Figure 22. The presently available hot firing data of conical and contoured nozzles separate earlier than predicted by Schilling. It can be supposed that Schilling used almost only cold flow data from small contoured nozzles, which, according to Figure 7, have a much lower separation pressure ratio.

Kalt-Bendall [35]. Kalt and Bendall used an expression of the form of equation (40) and fitted the constants to the available data of cold flow nozzles and hot firing tests with solid and liquid propellants. This resulted in

$$p_i/p_a = k_{KB_1} (p_c/p_a)^{k_{KB_2}} \tag{41}$$

$$= K_{in_{KB}} \quad , \tag{41a}$$

where

$$k_{KB_1} = 0.667$$

and

$$k_{KB_2} = -1.20 \quad .$$

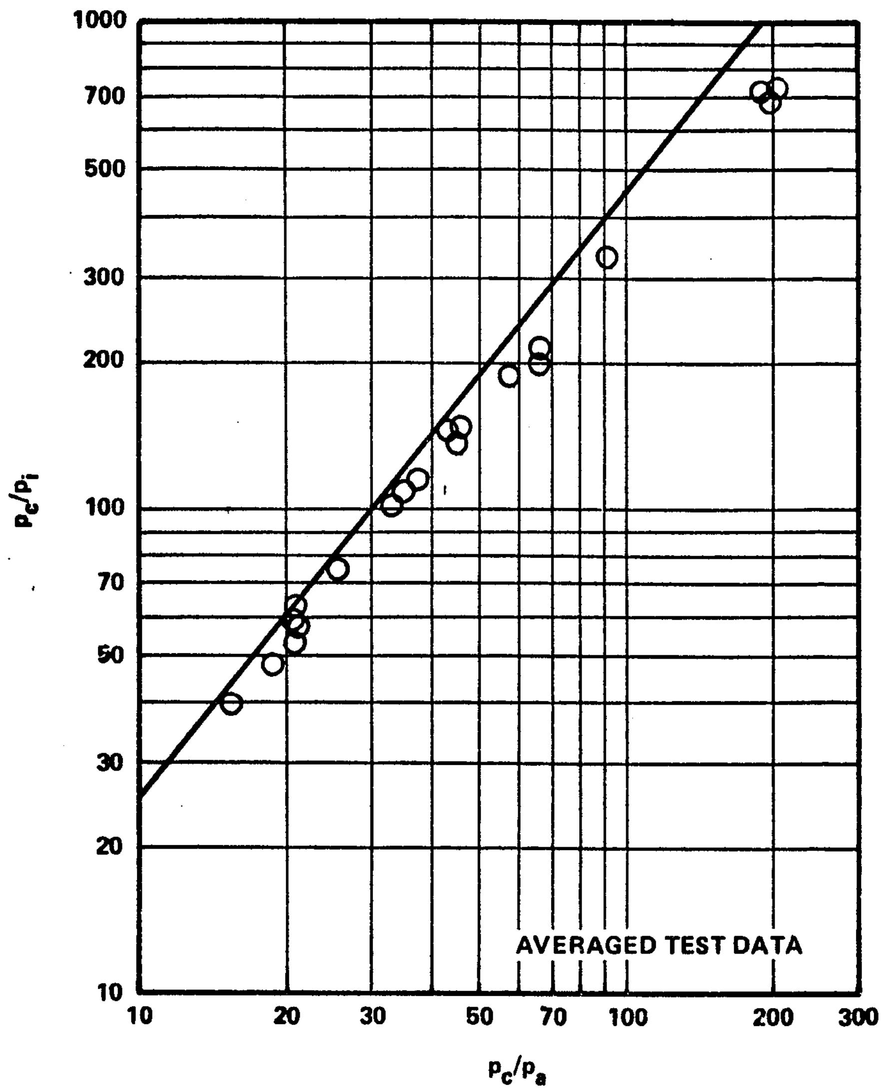

Figure 22. Schilling's separation criterion.

For comparison purposes, equation (41) is presented in Figure 23 in the same way as Schilling's equation. Clearly, the agreement with test data is better than it was in the case of Schilling, especially at lower pressure ratios. But at higher pressure ratios, a significant deviation from the test data is observed. All equations which are linear in logarithmic scale appear to decrease the separation criterion excessively at higher pressure ratios.

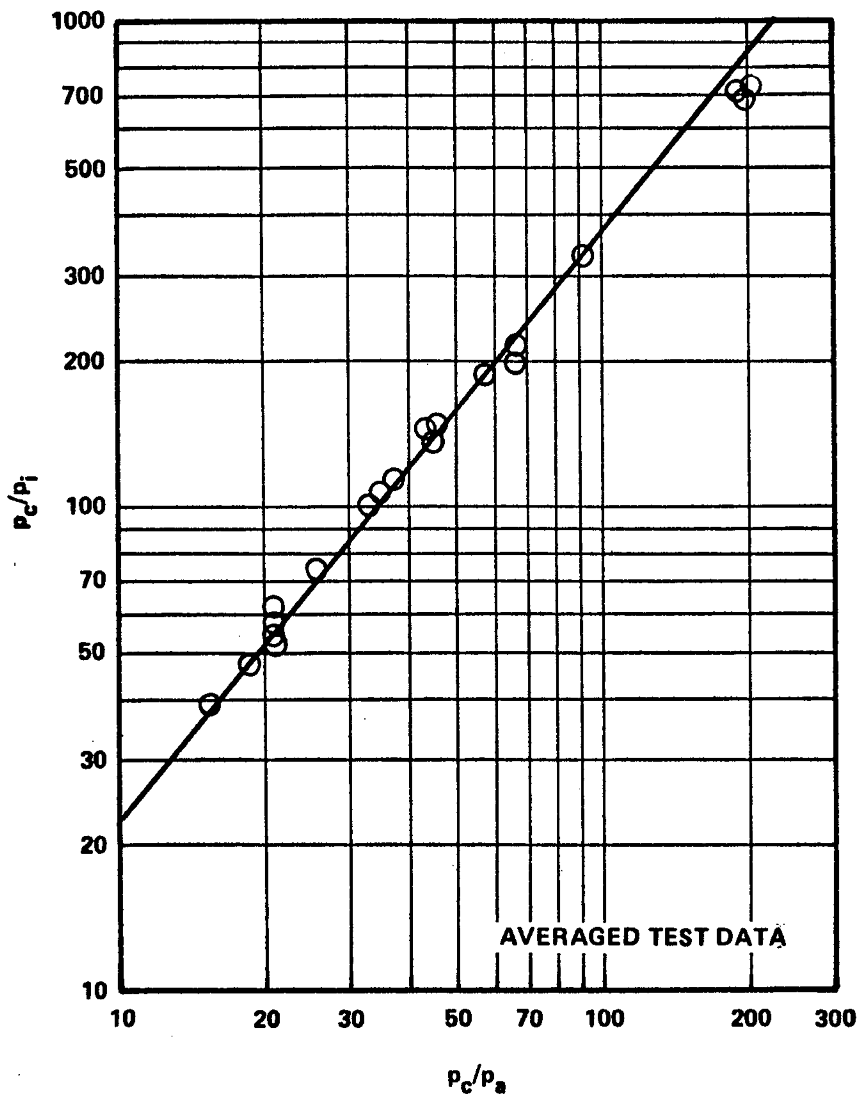

Figure 23. Kalt-Bendall's separation criterion.

Summary of Flow Separation Prediction Methods

Various relations are available in the literature which intend to predict the pressure rise in an overexpanded rocket nozzle with separation. The theoretical methods use a flat plate approach with zero pressure gradient. No improvement has been made by introducing a pressure gradient or a nozzle curvature. Therefore all theoretical results do not distinguish between small and large, conical and contoured nozzles. All theoretical methods depend on some empirical constants. They indicate a dependence of the separation criterion with the Mach number. Only the theory by Tyler-Shapiro results in a decrease of the separation criterion at higher Mach numbers [36]. Those theories which use only one empirical constant show a rather large dependence of the separation criterion on the isentropic exponent. Only the theory by Crocco-Probstein, which uses two constants, has an almost unvarying trend with changing γ. The wholly empirical correlations do not predict the experimental data well, but there is no reason that better empirical relations cannot be achieved.

Presently, three methods for flow separation prediction seem to give the best results:

1. Crocco-Probstein's separation theory with proper constants.

2. Graphical estimation of the separation criterion from Figure 8.

3. Reshotko-Tucker's Mach number ratio with $k_{RTL} = 0.762$ and $\gamma = 1.4$.

CONCLUSION

Flow separation data from hot firing nozzles with liquid propellants were collected from various sources to achieve a more general view of this problem. The presently available data favor the suggestion that small contoured nozzles exhibit a slightly different separation behavior than conical or larger bell shaped nozzles. In the latter case, the nozzle wall curvature is much smaller than in small contoured nozzles so that the centripetal forces due to flow deflection are more likely to be neglected.

Medium and large contoured nozzles and conical nozzles agree very well in the separation pressure ratio numbers. The nozzles show only a slight change of the separation behavior with Mach numbers. All other effects are more or less masked by the measurement errors.

Many different flow separation prediction methods have been published and can be divided into theoretical approaches and pure empirical correlations. Of these, the method developed by Crocco and Probstein leads to the best agreement between theory and experiment, with proper empirical constants. Using only a graphical representation of the various separation measurements, the separation characteristic of a selected nozzle design can easily be obtained.

APPENDIX

HOT FIRING SEPARATION DATA

The following nomenclature is used for the description of the nominal engine data which are contained in Tables A-1 through A-10.

$p_{c\ nom}$	design chamber pressure		
F_{nom}	design thrust		
ϵ	expansion ratio		
Θ	nozzle angle (b for bell nozzle)		
W	wall surface:	s	smooth wall
		t	tube wall
T	wall temperature:	u	uncooled
		c	cooled
		cc	cryogenically cooled

TABLE A-1. JET PROPULSION LABORATORY (FORSTER AND COWLES): 0.75K-ENGINE, HNO_3/ANILINE PROPELLANTS

Nominal Engine Data						Separation Data							Remarks
$p_{c\ nom}$ (N/cm²)	F_{nom} (N)	ϵ	Θ (deg)	W	T	p_i (N/cm²)	Δp_i ± (N/cm²)	p_a (N/cm²)	p_i/p_a	p_c (N/cm²)	ϵ_i	M_i	
200	3300	10	15	s	c	3.3	-	9.7	0.349	206	8	3.16	
						3.4		9.6	0.352	208	8	3.16	
						3.4		9.6	0.348	208	8	3.17	
						3.6		9.7	0.370	140	6	2.94	
						3.8		9.7	0.394	148	6	2.94	
						3.7		9.7	0.382	176	7	3.04	
						3.5		9.7	0.363	203	7	3.17	
						3.3		9.6	0.346	203	7	3.20	
						3.4		9.6	0.357	204	7	3.18	
						3.5		9.6	0.363	206	7	3.18	
						3.5		9.6	0.362	222	8	3.22	
						3.3		9.7	0.337	240	8	3.30	
						3.3		9.6	0.348	245	8	3.30	
		20.8				3.8		9.6	0.395	114	5	2.79	
						3.8		9.6	0.399	139	5	2.90	
						3.5		9.6	0.366	176	7	3.08	
						3.3		9.6	0.338	210	8	3.23	
						3.1		9.6	0.317	247	9	3.36	
						3.1		9.6	0.323	254	9	3.36	
		10	10			3.5		9.7	0.366	131	6	2.92	
						3.4		9.7	0.350	169	7	3.03	
						3.3		9.7	0.337	203	8	3.21	
						3.2		9.7	0.332	241	9	3.31	
		10	20	s	c	4.0		9.6	0.411	131	6	2.86	
						3.7		9.6	0.384	171	7	3.04	
						3.4		9.5	0.366	206	8	3.16	
						3.6		9.6	0.377	203	8	3.16	
						3.5		9.6	0.358	235	9	3.26	
						3.3		9.5	0.351	237	9	3.28	
		10	30			3.7		9.6	0.385	137	6	2.91	
						3.6		9.6	0.374	139	6	2.94	
						3.6		9.6	0.377	173	6	3.06	
						3.4		9.6	0.352	212	8	3.21	
						3.4		9.6	0.351	246	9	3.30	

TABLE A-2. NASA-LEWIS RC (BLOOMER ET AL.): 3K-ENGINE, O_2/KEROSENE PROPELLANT

Nominal Engine Data						Separation Data							Remarks
$p_{c\ nom}$ (N/cm^2)	F_{nom} (N)	ϵ	Θ (deg)	W	T	p_i (N/cm^2)	$\Delta p_i \pm$ (N/cm^2)	p_a (N/cm^2)	p_i/p_a	p_c (N/cm^2)	ϵ_i	M_i	
220	13000	50	20	s	c	0.33	0.1	1.23	0.279	223	46	4.58	
						0.62		2.18	0.286	224	32	4.20	
						1.1		3.7	0.287	223	20	3.88	
						1.48		5.2	0.285	223	16	3.69	
						0.33		1.23	0.268	220	48	4.58	
						0.82		3.18	0.263	222	24	4.02	
						1.3		4.2	0.313	221	16	3.74	
						1.5		5.2	0.295	220	14	3.67	
		42	25			0.51		1.74	0.291	220	32	4.32	
						0.76		2.7	0.281	217	27	4.07	
						1.1		3.7	0.300	218	21	3.86	
						1.44		4.7	0.305	217	16	3.70	
						0.51		1.72	0.291	209	33	4.29	
						0.76		2.7	0.277	210	27	4.05	
						1.11		3.7	0.304	215	21	3.84	
						1.4		4.7	0.297	210	16	3.69	
		75	25			0.31		1.14	0.271	220	69	4.62	
									0.283		32	4.30	
						1.03		3.6	0.282	218	21	3.90	
						1.47		5.1	0.290	210	16	3.67	
						0.28		1.01	0.277	216	66	4.67	
						0.53		2.03	0.262	214	30	4.27	
						1.16		3.7	0.313	214	21	3.82	
						1.5		5.1	0.296	214	15	3.67	
		60	30			0.43		1.66	0.260	216	53	4.41	
						0.71		2.6	0.267	215	32	4.10	
						0.48		1.7	0.289	216	39	4.35	
						0.68		2.6	0.260	213	31	4.12	
						1.1		3.8	0.291	210	21	3.84	
						1.5		4.7	0.316	210	16	3.67	

TABLE A-3. BRISTOL-SIDDLEY (SUNNLEY AND FERRIMAN): GAMMA ENGINE, H_2O_2/KEROSENE PROPELLANTS

Nominal Engine Data						Separation Data							Remarks
$p_{c\ nom}$[a] (N/cm^2)	F_{nom}[a] (N)	ϵ	Θ	W	T	p_i (N/cm^2)	Δp_i ± (N/cm^2)	p_a (N/cm^2)	p_i/p_a	p_c (N/cm^2)	ϵ_i	M_i	
370	22 000	10	17°	t	c	3.9	-	9.7	0.392	147	6	2.89	
						3.5		9.7	0.364	161	6	2.98	
						3.7		9.7	0.377	220	8	3.12	
						3.5		9.7	0.357	224	8	3.17	
220	89 000	14	17°	t	c	3.7		9.9	0.370	219	8	3.13	
						3.5		9.9	0.357	238	9	3.19	
						3.5		9.9	0.345	264	10	3.26	

a. Estimated Values

TABLE A-4. ROCKETDYNE: ATLAS SUSTAINER ENGINE (CONICAL NOZZLE) O_2/KEROSENE PROPELLANTS

Nominal Engine Data						Separation Data							Remarks
$p_{c\ nom}$ (N/cm²)	F_{nom} (N)	ϵ	Θ	W	T	p_i (N/cm²)	$\Delta p_i \pm$ (N/cm²)	p_a (N/cm²)	p_i/p_a	p_c (N/cm²)	ϵ_i	M_i	
400	270 000	25	15°	t	c	3.3	0.2	9.4	0.352	347	14	3.51	
						3.2		9.4	0.338	322	14	3.48	
						3.2		9.4	0.338	315	14	3.47	
						3.0		9.4	0.322	305	14	3.48	

TABLE A-5. ROCKETDYNE: J-2S ENGINE, O_2/H_2 PROPELLANTS

Nominal Engine Data						Separation Data							Remarks
$p_{c\ nom}$ (N/cm²)	F_{nom} (N)	ϵ	Θ	W	T	p_i (N/cm²)	$\Delta p_i \pm$ (N/cm²)	p_a (N/cm²)	p_i/p_a	p_c (N/cm²)	ϵ_i	M_i	
820	1 200 000	40	b	t	c	3.2	-	9.7	0.327	647	40	3.90	no side loads

TABLE A-6. ROCKETDYNE: J-2 ENGINE, O_2/H_2 PROPELLANTS

Nominal Engine Data						Separation Data							
$p_{c\,nom}$ (N/cm^2)	F_{nom} (N)	ϵ	Θ	W	T	p_i (N/cm^2)	$\Delta p_i \pm$ (N/cm^2)	p_a (N/cm^2)	p_i/p_a	p_c (N/cm^2)	ϵ_i	M_i	Remarks
450	1 000 000	27	b	t	c	3.9	0.3	9.8	0.402	210	9	3.12	transient data (NASA-MSFC measurements)
						3.4	0.2	9.8	0.346	332	15	3.48	
						3.3	0.1	9.8	0.333	400	18	3.61	
						3.1		9.8	0.321	392	18	3.62	
						3.2		9.8	0.323	393	18	3.62	
						3.1		9.8	0.321	391	18	3.62	
						3.1		9.8	0.315	415	20	3.66	
						3.0		9.8	0.309	405	22	3.66	
						3.8	0.3	9.8	0.379	200	9	3.13	
						3.8	0.3	9.8	0.380	201	9	3.13	
						3.3	-	9.8	0.338	450		3.68	no side loads

TABLE A-7. ROCKETDYNE: J-2 MODEL ENGINE, O_2/H_2 PROPELLANTS

Nominal Engine Data						Separation Data							Remarks
$p_{c\,nom}$ (N/cm^2)	F_{nom} (N)	ϵ	Θ	W	T	p_i (N/cm^2)	$\Delta p_i \pm$ (N/cm^2)	p_a (N/cm^2)	p_i/p_a	p_c (N/cm^2)	ϵ_i	M_i	
450		27.5	b	s	c	2.5	0.2	9.4	0.272	278	15	3.55	unpub-
						2.7		9.4	0.288	287	16	3.52	lished
						2.4		9.4	0.252	296	17	3.62	data
						2.3		9.4	0.248	299	19	3.64	
						2.1		9.4	0.224	303	25	3.70	
						2.5		9.4	0.271	342	26	3.66	
						2.5		9.4	0.269	341	26	3.66	
						2.3		9.4	0.246	317	26	3.68	
						2.3		9.4	0.243	315	25	3.68	
						2.2		9.4	0.230	303	24	3.69	

TABLE A-8. PRATT & WHITNEY AIRCRAFT: RL-10 ENGINE, O_2/H_2 PROPELLANTS

Nominal Engine Data						Separation Data							Remarks
$p_{c\,nom}$ (N/cm^2)	F_{nom} (N)	ϵ	Θ	W	T	p_i (N/cm^2)	$\Delta p_i \pm$ (N/cm^2)	p_a (N/cm^2)	p_i/p_a	p_c (N/cm^2)	ϵ_i	M_i	
200	67 000	67	b	t	c	3.7	-	10	0.367	204	-	3.15	
						0.95	0.2	3.06	0.311	204	28	3.95	

TABLE A-9. PRATT & WHITNEY AIRCRAFT: HIGH PRESSURE ENGINE, O_2/H_2 PROPELLANTS

Nominal Engine Data						Separation Data							
$p_{c\,nom}$ (N/cm^2)	F_{nom} (N)	ϵ	Θ	W	T	p_i (N/cm^2)	Δp_i ± (N/cm^2)	p_a (N/cm^2)	p_i/p_a	p_c (N/cm^2)	ϵ_i	M_i	Remarks
2040	44 000	205	b	s	u	2.9	0.5	10	0.286	2050	112	4.71	short
		250				2.9		10	0.286	2050	116	4.71	duration
		250				3.1		10	0.306	2080	110	4.67	tests
		250				2.4		10	0.245	1990	123	4.79	
		125				3.3		10	0.327	2100	102	4.64	
2040	44 000	100	b	s	u	2.4	0.3	10	0.245	1970	94	4.78	short
						3.0		10	0.299	2030	81	4.67	duration
						2.7		10	0.272	1930	87	4.70	tests
						3.1		10	0.306	2030	80	4.66	
						2.8		10	0.279	1950	86	4.69	
						3.0		10	0.299	2060	81	4.68	
		99				3.0		10	0.299	2100	81	4.69	

TABLE A-10. PRATT & WHITNEY AIRCRAFT: SPACE SHUTTLE MAIN ENGINE MODEL (BOOSTER, ORBITER, BASELINE), O_2/H_2 PROPELLANTS

Nominal Engine Data						Separation Data							Remarks
$p_{c\ nom}$ (N/cm^2)	F_{nom} (N)	ϵ	Θ	W	T	p_i (N/cm^2)	$\Delta p_i \pm$ (N/cm^2)	p_a (N/cm^2)	p_i/p_a	p_c (N/cm^2)	ϵ_i	M_i	
340	900	35	b	s	c	2.2	0.3	10	0.219	219	12	3.50	
						2.1		10	0.214	284	17	3.65	
						2.2		10	0.221	352	21	3.78	
						2.2		10	0.221	416	26	3.88	
		35	b	s	c	1.7		10	0.175	208	17	3.60	
						1.8		10	0.184	270	20	3.72	
						2.2		10	0.223	338	21	3.74	
						2.4		10	0.241	400	22	3.80	
		80	b	s	c	3.0		10	0.299	213	8	3.30	
						3.0		10	0.301	274	11	3.56	
						2.2		10	0.221	339	18	3.75	

TABLE A-11. NASA-MSFC: 4K-ENGINE, O_2/H_2 PROPELLANTS

Nominal Engine Data						Separation Data							Remarks
$p_{c\ nom}$ (N/cm^2)	F_{nom} (N)	ϵ	Θ	W	T	p_i (N/cm^2)	$\Delta p_i \pm$ (N/cm^2)	p_a (N/cm^2)	p_i/p_a	p_c (N/cm^2)	ϵ_i	M_i	
680	1800	20	18°	s	u	2.9	0.1	9.7	0.295	460	17	3.75	
						3.0		9.7	0.303	423	16	3.71	

REFERENCES

1. Lawrence, R.A.: Symmetrical and Unsymmetrical Flow Separation in Supersonic Nozzles. Ph.D. Thesis, Southern Methodist University, Texas, 1967.

2. Stodola, A.: Steam and Gas Turbines. McGraw-Hill Book Company, New York, 1927.

3. Summerfield, M.; Forster, C.; and Swan, W.: Flow Separation in Overexpanded Supersonic Exhaust Nozzles. vol. 24, Jet Propulsion Lab, Sept. 1954, pp. 319-320.

4. Barrere, M. et al.: Rocket Propulsion. Elsevier Publishing Company, New York, 1961.

5. Sutton, G.P.: Rocket Propulsion Elements. John Wiley and Sons, New York, 1967.

6. Moriarty, M.P.: J-2S Engine J116-D with Baffled Injector (U/N 616) - Side-Load Test Series. Rocketdyne Report CDR 2124-4004, July 20, 1972.

7. Herbert, M.V. and Herd, R.J.: Boundary Layer Separation in Supersonic Propelling Nozzles. Ministry of Aviation, Reports and Memoranda No. 3421.

8. Nave, L.H.: Evaluation of the Nozzle Incipient Separation Chamber Pressure for the SSME 470K Engine. Rocketdyne Report, Dec. 1, 1972.

9. Stromsta, R.R.: Results of J-2SE 40:1 Area-Ratio Bell Nozzle Design and Cold-Flow Test Program. Rocketdyne Report LAP 67-368(RC), Aug. 31, 1967.

10. Thayer, E.B. and Booz, D.E.: Flow Separation Tests of Candidate Space Shuttle Nozzles. SMR FR-3491, Pratt & Whitney Aircraft, Nov. 21, 1969.

11. Shapiro, A.H.: The Dynamics and Thermodynamics of Compressible Fluid Flow. Vols. 1 and 2, The Ronald Press Company, New York, 1954.

12. Sunley, H. L. and Ferriman, V. N.: Jet Separation in Conical Nozzles. Journal of the Royal Aeronautical Society, vol. 68, 1964, pp. 808-817.

13. Bloomer, H. J.; Antl, R. J.; and Renas, P. E.: Experimental Study of Effects of Geometric Variables on Performance of Conical Rocket Engine Exhaust Nozzles. NASA TN D-846, 1961.

14. Forster, C. R. and Cowles, F. B.: Experimental Study of Gas-Flow Separation in Overexpanded Exhaust Nozzles for Rocket Motors. JPL, Progress Report No. 4-103, 1949.

15. Kah, C. L. and Lewis, C. D.: High Chamber Pressure Staged Combustion Research Program, Final Report. FR-1676, Pratt & Whitney Aircraft, June 30, 1966.

16. Schilling, T. W.: Flow Separation in a Rocket Nozzle. M. S. Thesis, University of Buffalo, June 1962.

17. Zuckrow, M.: Aircraft and Missile Propulsion. John Wiley and Sons, New York, 1963.

18. Ahlberg, J. H.; Hamilton, S.; Migdal, D.; and Nilson, E. N.: Truncated Perfect Nozzles in Optimum Nozzle Design. ARS-Journal, vol. 31, no. 5, May 1961, pp. 614-620.

19. Campbell, C. E. and Farley, J. M.: Performance of Several Conical Convergent-Divergent Rocket Type Exhaust Nozzles. NASA TN D-467.

20. Chapman, D. R.; Kuehn, D. M.; and Larson, H. K.: Investigation of Separated Flows in Supersonic and Subsonic Streams With Emphasis on Effect of Transition. NACA TN 3869, 1957.

21. Farley, J.M. and Campbell, C. E.: Performance of Several Methods of Characteristics Exhaust Nozzles. NASA TN D-293.

22. Pratt & Whitney Aircraft: Suggested Program for Applied Research on Nozzle Flow Separation. PWA FP 65-117, 1966.

23. Donaldson, C. du and Lange, R.H.: Study of Pressure Rise Across Shock Waves Required to Separate Laminar and Turbulent Boundary Layers. NACA TN 2770.

24. Elkstroem, A.: Incipient Separation at Supersonic and Hypersonic Speeds. UTSI, Short Course on Flow Separation, 1972.

25. Mager, A.: Prediction of Shock Induced Turbulent Boundary Layer Separation. Journal of the Aeronautical Sciences, vol. 22, no. 3, Mar. 1955, pp. 201-202.

26. Mager, A.: On the Model of the Free, Shock Separated Turbulent Boundary Layer. Journal of the Aeronautical Sciences, vol. 23, no. 2, Feb. 1956, pp. 181-184.

27. Reshotko, E. and Tucker, M.: Effect of a Discontinuity on Turbulent Boundary Layer Thickness Parameters and Application to Shock-Induced Separation. NACA TN 3454, May 1955.

28. Gruman, W.J.: On the Plateau and Peak Pressure of Regions of Pure Laminar and Fully Turbulent Separation in Two Dimensional Flow. Journal of the Aeronatuical Sciences, vol. 26, no. 1, 1959, p. 56.

29. Lawrence, R.A. and Weynand, E.: Factors Affecting Flow Separation in Contoured Supersonic Nozzles. AIAA Journal, vol. 6, June 1968, pp. 1159-1160.

30. Crocco, L. and Probstein, R.F.: The Peak Pressure Rise Across an Oblique Shock Emerging From a Turbulent Boundary Layer Over a Plane Surface. Report 254, Princeton University, Mar. 1954.

31. Crocco, L. and Lees, L.: A Mixing Theory For the Interaction Between Dissipative Flows and Nearly Isentropic Streams. Journal of the Aeronautical Sciences, vol. 19, no. 10, Oct. 1952, pp. 649-676.

32. Arens, N. and Spiegler, E.: Shock Induced Boundary Layer Separation in Overexpanded Conical Exhaust Nozzles. AIAA Journal, vol. 1, no. 3, Mar. 1963, pp. 578-581.

REFERENCES (Concluded)

33. Arens, M.: The Shock Position in Overexpanded Nozzles. Journal of the Royal Aeronautical Society, vol. 67, 1963, pp. 268-269.

34. Gadd, G. E.: Interactions Between Wholly Laminar and Wholly Turbulent Boundary Layers and Shock Waves Strong Enough to Cause Separation. Journal of the Aeronautical Sciences, vol. 20, 1953, pp. 729-739.

35. Kalt, S. and Bendal, D.: Conical Rocket Nozzle Performance Under Flow Separated Conditions. Journal of Spacecrafts and Rockets, vol. 2, no. 3, May 1965, pp. 447-449.

36. Tyler, R. D. and Shapiro, A. H.: Pressure Rise Required for Separation in Interaction Between Turbulent Boundary Layer and Shock Wave. Journal of the Aeronautical Sciences, vol. 20, no. 12, Dec. 1953, pp. 858-860.

37. Hege, D. W.: Semi-Annual Technical Program Report, Atlas. Rocketdyne Report R-354-1P [AF04(645)-1], Dec. 30, 1956.

38. Lewis, J. T.: Results of Separated Nozzle Flow Studies on E-6 and E-7 Engine Stands. Pratt & Whitney Aircraft, FR-SMR, Feb. 8, 1967.

39. Kah, C. L. and Lewis, G. D.: High Pressure Rocket Engine Feasibility Program. Pratt & Whitney Aircraft, FR-1171, Dec. 10, 1964.

BIBLIOGRAPHY

Arens, M.: Turbulent Shock Wave Boundary Layer Separation and Overexpanded Nozzle Flow. LAF Congress No. 13, Varna Bulgaria.

Arens, M.: Flow Separation in Overexpanded Contoured Nozzles. AIAA Journal, vol. 1, no. 8, Aug. 1963, pp. 1945-1946.

Green, J., Jr.: Flow Separation in Rocket Nozzles. ARS Journal, vol. 23, Jan.-Feb. 1953, pp. 34-35.

Lange, R. H.: Present Status of Information Relative to the Prediction of Shock Induced Boundary Layer Separation. NACA, TN 3065.

APPROVAL

STATUS OF FLOW SEPARATION PREDICTION IN LIQUID PROPELLANT ROCKET NOZZLES

By Robert H. Schmucker

The information in this report has been reviewed for security classification. Review of any information concerning Department of Defense or Atomic Energy Commission programs has been made by the MSFC Security Classification Officer. This report, in its entirety, has been determined to be unclassified.

This document has also been reviewed and approved for technical accuracy.

O. K. GOETZ
Chief, Turbomachinery and Combustion Devices Branch

J. A. LOMBARDO
Deputy Chief, Propulsion Division

A. A. McCOOL
Director, Structures and Propulsion Laboratory

☆U.S. GOVERMENT PRINTING OFFICE 1974 – 640-448 / 165 REGION NO. 4